The Roles of *Flrt2* and *Flrt3* Cell Surface Proteins during Mouse Development



Ahmed Salman

Sir William Dunn School of Pathology

and

Brasenose College

This thesis was submitted as part of the requirement for the degree of Masters of Science by research in pathology

University of Oxford, Trinity Term 2012

Supervisor: Prof. Elizabeth Robertson

Declaration

‘I hereby declare that this submission is my own work and to the best of my knowledge it contains no materials previously published or written by another person, or substantial proportions of material which have been accepted for the award of any other degree or diploma at the University of Oxford or any other educational institution, except where due acknowledgement is made in the thesis. Any contribution made to the research by others, with whom I have worked at the University of Oxford or elsewhere, is explicitly acknowledged in the thesis. I also declare that the intellectual content of this thesis is the product of my own work, except to the extent that assistance from others in the project's design and conception or in style, presentation and linguistic expression is acknowledged.’

Signed

Date 25th December 2012

Acknowledgements

I would first like to thanks my supervisors, Professor Elizabeth Robertson and Professor Elizabeth Bikoff for their continuous support and encouragement throughout this poject.

I would also like to thanks all members of the Robertson/Bikoff lab for the help, support and valuable advice in matters related to the work shown in this thesis. Particularly Dr. Kim Cheng, for the help with editing the manuscript and technical issues related to the work, and Dr. Wei-Yuan Yu for the help with the experimental design and histology. Thanks to all the staff in the Dunn school of Pathology for their great help and support.

Finally, I must not forget to thank my wife, my parents, my family and friends outside the lab for their support and encouragement, without them I wouldn't be able to continue with the same enthusiasm.

Abbreviations

AER – Apical ectodermal ridge

ADE – Anterior definitive endoderm

A-P – Anterior posterior

AS – Anterior somite

AVE – Anterior visceral endoderm

BM – Basement membrane

BMP – Bone morphogenesis protein

CA – Conditional allele

CDS – Coding sequence

Ch – Chorion

$COONH_2$ – C- terminal

DE – Definitive endoderm

DNA – Deoxyribonucleic acid

drg – Dorsal root ganglia

ds RNA – Double stranded RNA

DTA – Diphtheria toxin A

D-V – Dorsal ventral

E – Embryonic day

EB – Embroyid body

ECO – Ectodomain

EDTA – Ethylenediaminetetraacetic acid

EMT – Epithelial-to-mesynchymal transition

ES – Embryonic stem

ESC – Embryonic stem cell

EUCOMM – European conditional mouse mutagenesis

KOMP – Knockout mouse project

FGF – Fibroblast growth factor

FLP – Flippase recognition target

Flrt – Fibronectin leucine-rich repeat transmembrane

FN – Fibronectin

FV – Fourth ventricle

GTPase – Guanosine triphosphatase

H – Heart

H&E – Hematoxylin and eosin

HL – Hindlimb

HYG – Hygromycin

ICM – Inner cell mass

IKMC – International knockout mouse consortium

IR – Intra-retinal space

IRES – Internal ribosomal entry site

L-R – Left right

LacZ – E. Coli beta-galactosidase

Lb – Limb

LoxP – Lox site called bacteriophage P1

LPHN – Latrophilin

LRR – Leucine-rich repeat

MA – Maxillary arch

MB – Midbrain

ME – Mesenchyme

mRNA – Messenger ribonucleic acid

MTP – Microsomal triglyceride transfer protein

N – Node

NE – Neural ectoderm

Neo – Neomycin

NH_2 –

NorCOMM – North American conditional mouse mutagenesis

P – Pancreas

PA – Pharyngeal arche

PBS – Phosphate buffered saline

PC – Pericardium

PCR – Polymerase chain reaction

P-D – Proximal dorsal

PEO – Pro-epicardial organ

PFA – Paraformaldehyde

Pdx.1 – Pancreatic and duodenal homeobox-1

PS – Primitive streak

RIP – Rat insulin promoter

RNA – Ribonucleic acid

S – Somite

Scx – Scleraxis

Sema3D – Semaphorin 3D

T – Telencephalon

TAE – Tris-acetate EDTA

TE – Trophectoderm

Tg – Transgene

TGF-β – Transforming growth factor beta

TIGM – Texas institute of genomic medicine

Tk – Thymidine kinase

TLR – Toll-like receptor

TM – Transmembrane

VE – Visceral endoderm

WISH – Whole embryo *in situ* hybridisation

WT – Wild type

x^2 – Chi square

X-gal – 5-bromo-4-chloro-3-indoyl beta-Dgalactopyranoside

ZPA – Zone of polarising activity

Abstract

Embryos morphogenesis relies on the interactions between different tissues and their constituent cells. These interactions are controlled by different signalling and adhesion molecules, such as the Fibronectin Leucine-rich Repeat transmembrane (Flrt) family of proteins. The closely related *Flrt2* and *Flrt3* share 45% amino acid sequence identity, and show several sites of co-expression in the developing mouse embryo. Experiments in this laboratory have shown that mice deficient in either one of *Flrt2* or *Flrt3* are embryonic lethal due to cardiac insufficiency, and structural defect in the AVE and a fusion failure of the lateral body walls of the embryo respectively. The highly conserved structural features shared between *Flrt2* and *Flrt3* suggest possible shared functional roles between the two closely related genes. The aims of this study were first to generate a *Flrt2* and *Flrt3* double mutant embryos, and examine the hypothesis that the two genes function cooperatively at sites of their co-expression. The second goal was to generate a *Flrt2 LacZ* reporter and a conditional alleles, using the EUCOMM/KOMP resource, to further analyse *Flrt2* expression patterns and function.

Flrt2 and *Flrt3* double mutant embryos were embryonic lethal at embryonic day (E) 10. The genetic experiment designed in this study suggests that *Flrt3* seems to function in cooperation with *Flrt2*, to maintain tissue integrity in the developing mouse embryo as loss of both exhibits a more severe phenotype than the single mutants, and has a more severe impact on the embryonic development.

The *Flrt2 LacZ* reporter and conditional alleles generated in this study were shown to be useful tools in dissecting *Flrt2* expression patterns, and can be used in further experiments to study the expression of *Flrt2* in particular sites

that have not been studied or extensively mentioned in the literature, or in site-specific deletion of *Flrt2* in tissues where *Flrt2* is expressed but the function has not been elucidated.

Contents

DECLARATION ..... **I**

ACKNOWLEDGEMENTS ..... **II**

ABSTRACT ..... **VI**

CONTENTS ..... **VIII**

CHAPTER 1

INTRODUCTION **1**

1.1 OVERVIEW OF EARLY MOUSE EMBRYONIC DEVELOPMENT 2

1.1.1 Morphogenesis and organogenesis of the mouse embryo 4

1.2 CELL ADHESION MOLECULES DURING EARLY MOUSE EMBRYONIC DEVELOPMENT 5

1.3 FIBRONECTIN LEUCINE-RICH REPEAT TRANSMEMBRANE PROTEINS 6

1.3.1 The role of Flrt family of proteins in mouse 7

1.3.2 The role of *Flrt3* in cell adhesion and tissue morphogenesis in the developing mouse embryo 11

1.3.3 The role of *Flrt2* in maintaining tissue integrity of the epicardium of the heart 13

1.4 AIMS OF THIS THESIS 15

CHAPTER 2 MATERIALS AND METHODS **16**

2.1 MATERIALS 17

2.1.1 Buffers and solutions 17

2.2 GENOMIC DNA ISOLATION FROM MOUSE EAR BIOPSY/EMBRYONIC TISSUES 18

2.3 POLYMERASE CHAIN REACTION (PCR) 18

2.4 GEL ELECTROPHORESIS 20

2.5 HISTOLOGY TECHNIQUES 20

2.5.1 Embryo harvesting and processing for paraffin sectioning 20

2.5.2 Hematoxylin and Eosin staining 20

2.5.3 X-gal staining 21

CHAPTER 3 GENERATION OF *FLRT2* AND *FLRT3* DOUBLE MUTANT EMBRYOS **22**

3.1 INTRODUCTION 23

3.2 RESULTS 25

3.2.1 Breeding strategies to generate *Flrt2* and *Flrt3* double mutant embryos 25

3.2.1.1 Generating *Flrt2*$^{+/-}$; *Flrt3*$^{CA/CA}$ female mice 25

3.2.1.2 Generating *Flrt2*$^{+/-}$; *Flrt3*$^{+/-}$; *Sox2 Cre* transgene mice 29

3.2.2 Generation of *Flrt2*$^{-/-}$; *Flrt3*$^{-/-}$ double mutant embryos 34

3.2.3 Recovery of *Flrt2*$^{-/-}$; *Flrt3*$^{-/-}$ embryos at E9.5 and E10.5 38

3.2.4 Conclusion 40

…**CHAPTER 4 GENERATION OF *FLRT2* REPORTER AND CONDITIONAL ALLELS** **43**

4.1 INTRODUCTION 44
4.2 RESULTS 47
4.2.1 Generating *Flrt2* reporter/conditional allele using targeting via ESC technology .. 47
4.2.2 PCR confirmation of the *Flrt2* EUCOMM/KOMP targeted allele 47
4.2.3 Generation of the *Flrt2* conditional mouse strain 48
4.2.4 Comparison of sites of *Flrt2* expression using the *Flrt2 LacZ* reporter mice 53
4.3 EXPRESSION OF *LACZ* PROTEIN IN THE DEVELOPING MOUSE EMBRYO 54
4.3.1 *Flrt2* promoter driven *LacZ* expression at E9.5 54
4.3.2 *Flrt2* promoter driven *LacZ* expression at E10.5 54
4.3.3 *Flrt2* promoter driven *LacZ* expression at E11.5 55
4.4 CONCLUSION 59

. CHAPTER 5 GENERAL DISCUSSION 61

5.1 INTRODUCTION 62
5.2 MICE LACKING *FLRT2* AND *FLRT3* WERE EMBRYONIC LETHAL 63
5.3 *FLRT2 LACZ* REPORTER AND *FLRT2* CONDITIONAL ALLELE ARE USEFUL TOOLS FOR DISSECTING *FLRT2* EXPRESSION DOMAINS 65
5.4 OUTLOOK AND FURTHER EXPERIMENTS 65

CHAPTER 6 REFERENCES 68

Chapter 1

Introduction

1.1 Overview of early mouse embryonic development

Early mouse embryonic development is a complex and sophisticated process. Our understanding of mouse developmental biology has been aided by the manipulation of mouse embryos and investigation of cell signalling pathways that determine cell fate during mouse embryonic development, in particular, with the development of embryonic stem (ES) cell and transgenic technology. In the last two decades comprehensive analysis of the main cellular and molecular processes underlying embryonic development has been investigated.

The gestational period for mice is three weeks and these three weeks can be divided into two main stages, pre-implantation and post-implantation. The pre-implantation stage describes the first five days of gestation during which the small (approximately 80 μm in diameter) fertilized egg undergoes a steady rate of cell division. In the first three days of embryonic development (E3), the mouse embryo will have reached the 16-cell stage. At E3.5 the fertilized egg becomes a blastocyst that comprises an inner cell mass (ICM), that subsequently forms the embryo, and an outer layer of cells called the trophectoderm (TE), which contribute to the extra-embryonic tissue (Beddington and Robertson, 1999). Implantation occurs at approximately E4.5 and this physical attachment leads to invasion and growth of the TE and eventually leading to the formation of placenta, where oxygen and nutrients are passed on from the mother to the embryo (Arnold and Robertson, 2009).

The next stage of development is described as the post-implantation stage. At approximately E5, the proximal and distal (P-D) body axis is established and the embryo can be divided into two distinct regions, the extraembryonic region that contributes to the formation of the placenta, and the epiblast-derived (tissue type derived from the ICM) embryonic region that

subsequently elongates along the P-D axis contributing to the formation of the embryo (Arnold and Robertson, 2009). These highly controlled morphological events are driven by signalling pathways including the TGF-β signalling pathway (Arnold and Robertson, 2009) .

After E5, the three main body axes of the mouse embryo begins to be specified; the anterior posterior axis (A-P) (Sundararajan et al., 2012), the dorsal ventral axis (D-V) and the left right axis (L-R). These events are coordinated via tightly controlled cellular and molecular biochemical pathways. Patterning of the axes is provided by specialised signalling centres that include the anterior visceral endoderm (AVE), node and notochord (Arnold and Robertson, 2009; Hackett, 2002; Nonaka et al., 2005). Failure to correctly establish the L-R body axis leads to severe morphological consequences, such as situs inversus, a syndrome in mouse and human where disruption of the orientation of the L-R axes causes the organs within the body cavity to be reversed (Hackett, 2002).

Up until E6 the mouse embryo consists of 2 layers, after which gastrulation occurs, when the three embryonic germ cell layers are established; the ectoderm, mesoderm and definitive endoderm (DE) (Arnold and Robertson, 2009). Gastrulation utilises a set of morphogenetic movements coupled with cell proliferation and differentiation during which the mouse embryo is converted from two germ layers into three (Tam and Behringer, 1997). Nodal, a member of TGF-β family of growth factors, is essential for gastrulation (Robertson et al., 2003). One of several events at the beginning of gastrulation that relies on Nodal/TGF-β signalling pathway is the formation of a structure called the primitive streak where mesoderm cells are specified (Varlet et al., 1997). The ectoderm forms the outer layer of the embryo, it arises from the embryonic

epiblast, and contributes to structures including the central nervous system (CNS), the epidermis, nail, hair and lens of the eye (Rathjen et al., 1999). The mesoderm is described as an additional layer between the ectoderm and the endoderm, it forms structures including the heart, vascular and connective tissues. Mesenchymal cells serve as precursors of diverse cell lineages including striated and smooth muscle cells, endothelial and connective tissue cells (De Langhe et al., 2008). Somite formation in the mouse embryo begins with the recruitment of mesenchymal cells into the paraxial mesoderm (Tam and Trainor, 1994). Somites give rise to the axial skeleton, muscles and dermis (Arnold and Robertson, 2009). The endoderm arises from the epiblast during gastrulation. The flattened cells, which subsequently become columnar, migrate inwards along the embryonic body forming the lining of the entire gut tube, except parts of the mouth and pharynx (which are lined by the ectoderm). It also forms the lining of all the glands that open into the digestive system, such as the lungs and salivary glands (Cascio and Zaret, 1991; Zaret, 2001).

1.1.1 Morphogenesis and organogenesis of the mouse embryo

The early post-implantation embryo undergoes a series of morphogenetic rearrangements following gastrulation, such as axis rotation and the inversion of the three germ layers. Each layer will contribute to specific part of the embryo body, for example, the ectoderm will form the outmost and the endoderm will form the innermost of the embryo body (Kaufmann, 1992). Between E6.5 and E8.5 limb buds, somites, neural tube and gut tube will differentiate and the ventral and dorsal body walls form. Between E8.5 and E10.5 the mouse embryo undergoes a series of morphological rearrangements including closure of the ventral and dorsal body wall and closure of the neural tube and gut tube

(Kaufman, 1992). By E12.5 the primitive heart has undergone looping morphogenesis and has four chambers with left and right atria and ventricles (Brand, 2003; Harvey, 1999, 2002).

1.2 Cell adhesion molecules during early mouse embryonic development

Embryo morphogenesis relies on the interplay between different tissues and the interaction between their constituent cells. Cell interactions are controlled by various molecules, such as signalling and adhesion molecules (Barone and Heisenberg, 2012). Throughout the process of gastrulation, cells of the developing embryo undergo a series of highly coordinated migration events that require cells to change their characteristic and behaviour. For example, at the onset of gastrulation at around E6, cells in the posterior epiblast form the mesoderm by undergoing an epithelial-to-mesenchymal transition (EMT). The EMT is a process where the cells change from one tissue type (epithelium) to another (mesenchyme) by loss of epithelial cell adhesion properties and epithelial cell polarity, subsequently causing the nascent mesoderm cells to delaminate from the primitive streak (PS) (Arnold and Robertson, 2009). The migration of the mesoderm cells from the posterior side of the embryo that occurs as a consequence of EMT of the nascent mesoderm, are just two of many migratory rearrangements of cells, tissues and germ layers that require changes in adhesion and cell to cell contact. These processes are crucial during mouse embryonic development.

1.3 Fibronectin leucine-rich repeat transmembrane proteins

The Fibronectin Leucine-rich Repeat Transmembrane (Flrt) protein family was initially identified in a screen for extracellular matrix (ECM) proteins expressed in human skeletal muscle (Lacy et al., 1999). They were subsequently identified as potential downstream targets of the Nodal/TGF-β/ signaling pathway in a *Xenopus* DNA microarray screen (Ogata et al., 2007). The Flrt protein family is a novel transmembrane type 1 family of proteins and is comprised of three proteins (Flrt 1-3). Each of the Flrt family of proteins contains ten extracellular leucine-rich repeats (LRRs) flanked by two cysteine- rich residues on the C- and N-terminal flanking regions, a fibronectin type-III domain (FN III), followed by a small transmembrane domain (Yamagishi et al.) and a highly conserved lysine residue at the short intracellular region (**Fig. 1.1**). The Flrt proteins are highly conserved, Flrt1 and Flrt3 are most similar in terms of homology, having 55% amino acid sequence identity and 16% similarity. Flrt2 and Flrt3 have 45% amino acid sequence identity and 20% similarity and Flrt1 and Flrt2 are 41% identical in amino acid sequence and 20% similar (Lacy et al., 1999).

The LRR region is one of the most important domains in the Flrt family of proteins. The LRRs are protein-ligand interaction motifs found in a large number of proteins of diverse structure, localisation and function in bacteria, fungi, plants and animals (Kobe and Kajava, 2001). The LRR motifs are arranged in different structures with a variable number of repeats. This structure of repetitive sequences of variable lengths generates a versatile and highly evolvable framework for the binding of diverse proteins and non-protein ligands (Dolan et al., 2007).

Seven different classes of LRRs have been identified so far and four different types have been described in mammals, three intracellular and one

extracellular (similar to the Flrt family) (Kajava, 1998; Kobe and Kajava, 2001). Each repeat is typically 19–29 amino acids long and has a well-conserved N-terminal stretch of 9–12 amino acids that is characterised by precisely positioned hydrophobic residues (usually leucine) (Dolan et al., 2007). The arrangement of multiple repeats in tandem generates a horseshoe-shaped solenoidal structure, which is important for protein-protein interaction between adjacent cells (**Fig. 1.2**).

1.3.1 The role of Flrt family of proteins in mouse

Orthologues of the Flrt family of proteins were previously identified and described in humans, as expressed in different tissues and organs like kidney, brain, skeletal muscles, brain heart, pancreas, lung, liver and placenta (Lacy et al., 1999). Flrts are also present in other model organisms such as rodents, and act as endogenous ligands involved in regulating the development of the central nervous system (O'Sullivan et al., 2012; Robinson et al., 2004; Yamagishi et al., 2011). In chick they are expressed during limb development (Smith and Tickle, 2006), whereas in frog, they have been shown to form a complex with Fibroblast growth factor (FGF) receptors to promote FGF signalling (Bottcher et al., 2004), and recently in zebrafish, as part of cell surface interacting network in the nervous system (Sollner and Wright, 2009). Expression patterns of Flrt1-3 proteins in mouse were first analysed by Haines and colleagues (Haines et al., 2006), and *Flrt1-3* were shown to have a functional role in regulating the FGF signalling pathway during mouse embryonic development (Haines et al., 2006). Fibroblast growth factors are mitogenic and chemotactic agents for a wide variety of cell types and play a primary role in the regulation of angiogenesis,

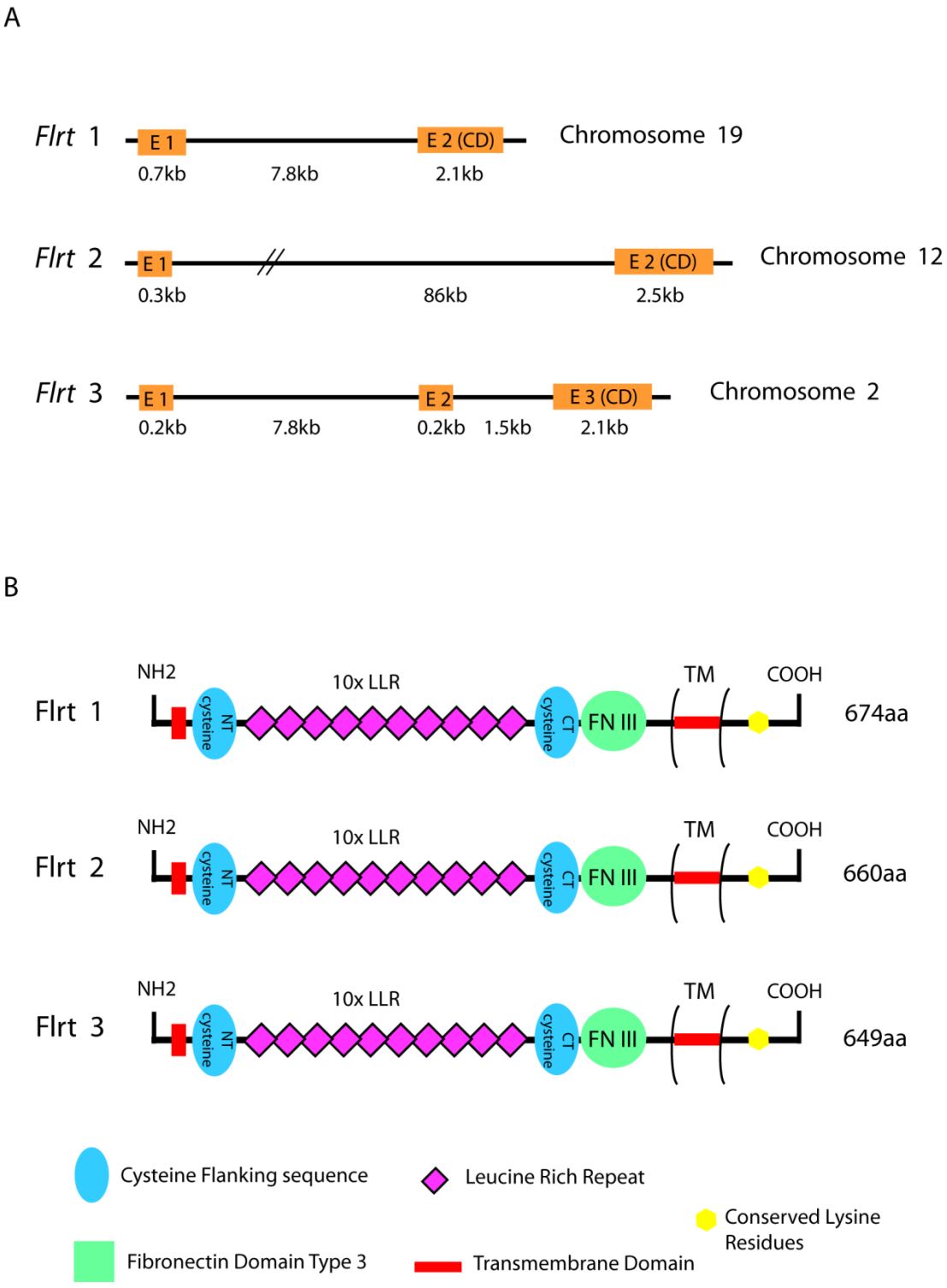
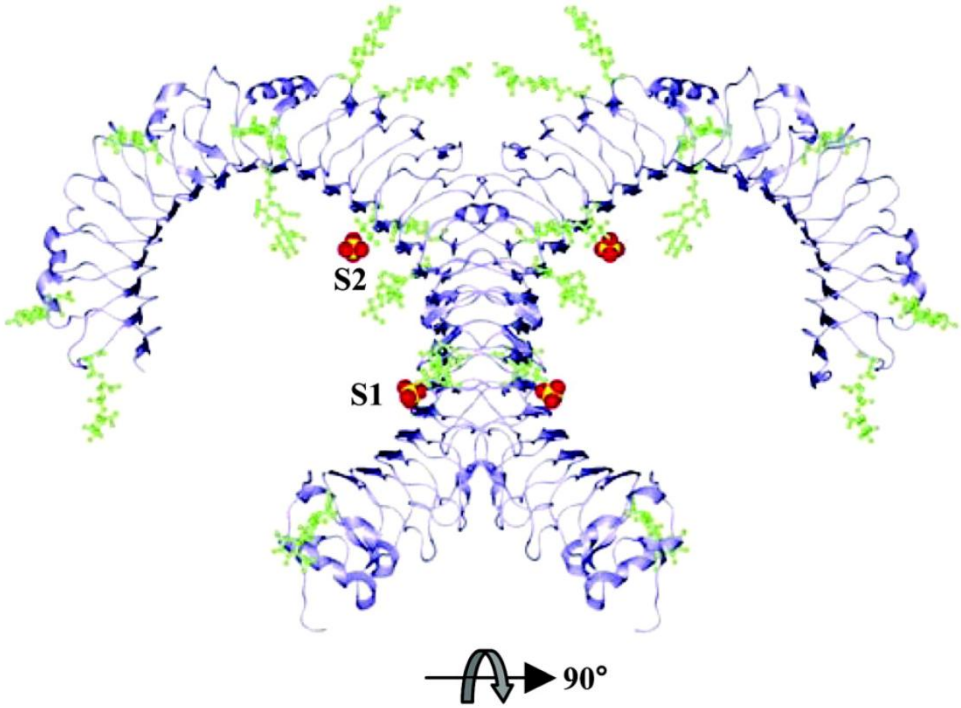


Figure 1.1, Genomic organisation and protein structure of the mouse Flrt family of proteins. (A) Schematic representation of the *Flrt1-3* genes showing their genomic position and organisation. All three genes have only one coding exon (the final exon). (B) Protein structure of the mouse Flrt family of proteins, the 10 LRRs (purple) are flanked by two cysteine-rich flanking regions (blue) followed by a transmembrane region (red) on the extracellular domain, and a short lysine rich intracellular region (yellow) on the C-terminal domain.



Taken from (Bell et al., 2005)

Figure 1.2. Leucine-rich repeat protein structure during dimerization. Using the Toll-like receptor type 3 (TLR3) homodimer as an example of the complex structure of the extracellular domains of LRR proteins, such as the Flrt family of proteins. This particular crystallised ectodomain (ECD) of human TLR3 dimer, with 23 LRRs each, recognises dsRNA, a molecular signature of viruses. The horseshoe-shaped protein core provides a large surface area for ligand interaction and recognition.

organogensis and wound healing (Blaber et al., 1996) suggesting that interaction with FGF signalling may be a general property of FLRT proteins.

It was previously reported that *Flrt3* is expressed during somite development and involved in a regulated migratory events in muscle precursor cells. *Flrt3* has also been shown to be expressed at the midbrain/hindbrain boundary (Haines et al., 2006), while *Flrt1* was observed at brain compartmental boundaries (Haines et al., 2006). *Flrt2* was described in the midbrain and has strong expression in an area of tissue posterior to the developing heart (Haines et al., 2006; Maretto et al., 2008; Muller et al., 2011), but no definite role of Flrt proteins has been described in these tissues.

It was not until experiments performed in this laboratory that early expression patterns of *Flrt1-3* were characterised (Maretto et al., 2008) (**Fig. 1.3**). All three members of the Flrt family were expressed during early mouse embryonic development but *Flrt3* was shown to be the most robust and expressed at the earliest time point (Maretto et al., 2008). At early stages of the mouse embryonic development *Flrt3* is expressed in the anterior visceral endoderm (AVE), which is an extra-embryonic tissue required for specifying anterior pattern in the mouse embryo (Rodriguez et al., 2005). As the mouse embryo develops, *Flrt3* was observed to be expressed at a number of sites including the somites, tissues ventral and caudal to the heart, the pharyngeal arches, brain, and limb buds (Maretto et al., 2008). Interestingly, *Flrt2* was shown to be co-expressed with *Flrt3* in the AVE, heart, somites, pharyngeal arches, brain, and limb buds (Maretto et al., 2008). Of the three members of the Flrt protein family, *Flrt1* expression was the most restricted, shown only to be expressed in the brain, limb buds, and dorsal root ganglia (Haines et al., 2006; Maretto et al., 2008).

1.3.2 The role of Flrt3 in cell adhesion and tissue morphogenesis in the developing mouse embryo

Flrt3 has been described on many previous occasions in the literature as having a diverse set of roles, however little is known regarding the *in vivo* function of Flrt1 and Flrt2. Recently, Flrt2 and Flrt3 were reported to bind to the Unc-5 receptor family of proteins, which are involved in various physiological interactions in the developing mammalian nervous system (Yamagishi et al., 2011). Interactions between Flrt2/3 and Unc-5D form ectodomains (ECDs) that act as a repulsive guidance for developing neurons. Flrt proteins have also been reported to act as endogenous ligands and regulate excitatory synapse development (O'Sullivan et al., 2012). O'Sullivan and colleagues showed that Flrt3 interacted with latrophilin3 (LPHN3), a member of the latrophilin G protein-coupled receptor family, to form ECDs that in turn reduced excitatory synapse density in cultured neurons. In addition, *Xenopus* Flrt3 has been reported to form a complex with FGF receptors (FGFRs) to activate intracellular signals, such as the canonical MAPK pathway, which results in ectopic tail formation (Bottcher et al., 2004). Flrt3 was also reported to regulate cell adhesion during gastrulation in *Xenopus* embryo by interacting with the small GTPase Rnd1 and this interaction is induced by Activin/Nodal TGF-β superfamily members (Ogata et al., 2007).

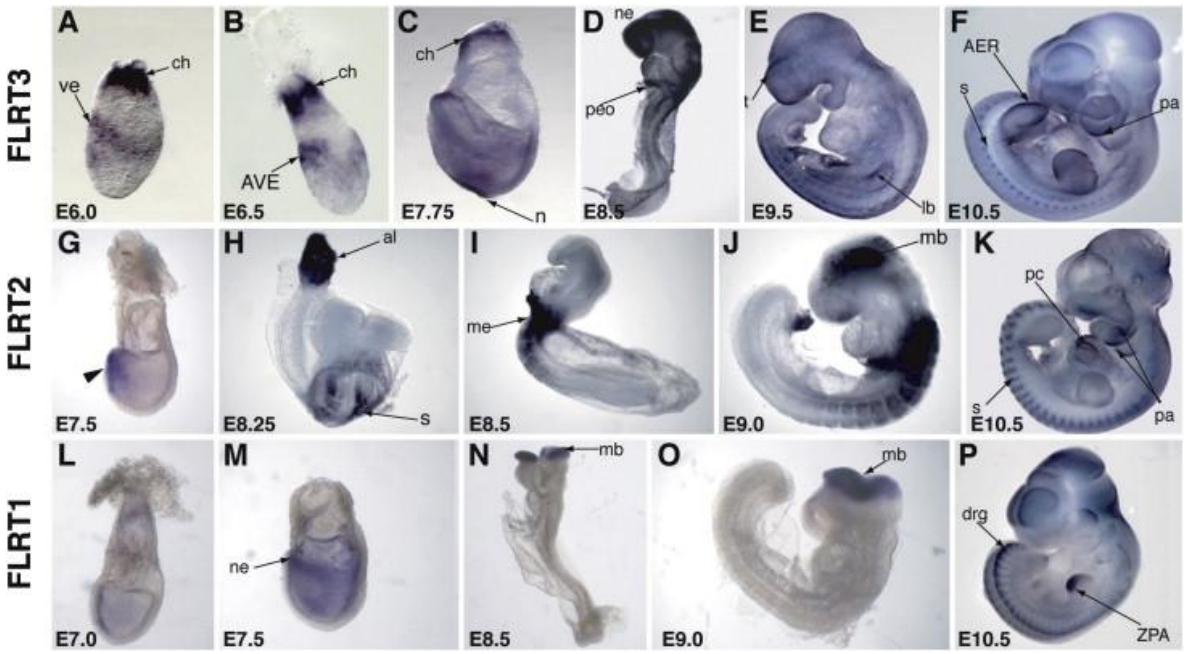


Figure as published in (Maretto et al., 2008)

Figure 1.3. Developmentally regulated expression of three fibronectin leucine-rich transmembrane genes FLRT1–3 at early post-implantation stages. (A–P) Whole mount *in situ* hybridization analysis of *FLRT1–3* expression. *FLRT3* mRNA is initially expressed at early streak stages in the AVE and the chorion (A and B). At early headfold stages *FLRT3* expression is maintained in the AVE and appears in the node and nascent definitive endoderm, and is down-regulated in the chorion (C). At E8.5 *FLRT3* is up-regulated in the headfolds, the somites and the proepicardial organ (D). From E9.5 onwards, *FLRT3* mRNA is present in the telencephalic vesicles, limb buds and the somites (E). At E10.5 *FLRT3* transcripts are detectable in the pharyngeal arches, the apical ectodermal ridge (AER) of the limb buds and the somites (F). *FLRT2* transcripts initially appear at mid-streak stages in the AVE and ADE tissue (arrowhead) (G). At E8.25 *FLRT2* expression is up-regulated in the most anterior somites and the allantois (H). Slightly later, at E8.5, *FLRT2* transcripts are strongly expressed in the trunk mesenchyme immediately caudal to the heart (I). At E9.0 *FLRT2* expression is detectable in the midbrain mesenchyme and the anterior somites (J). At E10.5 *FLRT2* is expressed in the pharyngeal arches and the somites (K). *FLRT1* initially shows ubiquitous weak expression at streak stages (L). At early headfold stages *FLRT1* is induced in the anterior neurectoderm (M). Between E8.5 and E9.0 strong expression is strictly confined to the forming midbrain (N, O). Slightly later at around E10.5, *FLRT1* expression is activated at additional sites, including the dorsal root ganglia and the ZPA of the limb buds (P). Abbreviations: AER, apical ectodermal ridge; al, allantois; AVE, anterior visceral endoderm; ch, chorion; drg, dorsal root ganglia; lb, limb buds; mb, midbrain; me, mesenchyme; n, node; ne, neural ectoderm; pa, pharyngeal arches; peo, proepicardial organ; pc, pericardium; s, somites; t, telencephalon; ve, visceral endoderm; ZPA, zone of polarizing activity

Although several phenotypic defects has been shown to be caused by deficiency in Flrt3, it is the defect in the integrity of the basement membrane of the AVE previously described that is most relevant for the purpose of this thesis (Egea et al., 2008; Maretto et al., 2008). The AVE secrets inhibitory signals that are essential for establishing the A-P axis of the developing mouse embryo (Lu et al., 2001; Perea-Gomez et al., 2002; Rossant and Tam, 2004).

Flrt3 was observed to be expressed in the AVE between E6 and E6.5 (Maretto et al., 2008) and *Flrt3*$^{-/-}$ embryos showed a highly disorganised basement membrane (BM) in the AVE region. The BM is critical for the development of the mouse embryo, and controls migration, differentiation and cell fate during early embryogenesis (Egea et al., 2008). The defect in the integrity of the BM results in holes in the surface of the AVE, exposing the epiblast underneath to the mesoderm inducing cues resulting in abnormal gastrulation (Egea et al., 2008; Maretto et al., 2008). In addition, *Flrt3*$^{-/-}$ embryos displayed defects in headfold fusion and failure of lateral edges of the ventral body wall to fuse, causing cardia bifidia and eventually death at E10.5, suggesting that Flrt3 may be required for tissue fusion (Maretto et al., 2008). In summary, embryos lacking Flrt3 were embryonic lethal due to defects in the AVE leading to pronounced anterior axis truncation and a delay in the migration of the AVE cells. This ultimately resulted in disorganisation of the A-P axis of the developing mouse embryo and death by E10.5 (Maretto et al., 2008).

1.3.3 The role of Flrt2 in maintaining tissue integrity of the epicardium of the heart

The pro-epicardial organ (PEO) is a cauliflower-like cluster of cells adjacent to the septum transversum (Manner et al., 2001). The septum transversum is a

tissue originating from the lateral plate mesoderm that contributes to the epicardium and diaphragm and promotes outgrowth of the liver (Rossi et al., 2001). The PEO itself gives rise to the epicardium (the outmost tissue layer that envelops the developing heart) that attaches and spreads across the surface of the myocardium (the middle layer of the heart) (Hiruma and Hirakow, 1989; Mikawa and Gourdie, 1996).

Flrt2 shows strong expression in the trunk mesenchyme underneath the developing heart in the mouse embryo (Maretto et al., 2008). Of particular interest, *Flrt2*$^{-/-}$ embryos displayed a very similar phenotype to mice lacking *Flrt3* in terms of disorganisation and loss of cell-cell contact in the epicardium and the AVE respectively. Mice lacking *Flrt2* displayed defects in the integrity of the epicardium and disturbances to the architecture of the underlying BM accompanied by a pronounced reduction in thickness of the ventricular myocardium (Muller et al., 2011). Meanwhile, mice lacking *Flrt3* display defect in the AVE and disorganisation of the underlying BM resulting in the exposure of the epiblast.

It was reported previously that *Flrt2* and *Flrt3* have overlapping expression domains including the pharyngeal arches, the developing heart, somites and central nervous system (Haines et al., 2006). Interestingly, *Flrt2* and *Flrt3* are both strongly expressed in the PEO (Muller et al., 2011). However, *Flrt3* is selectively downregulated following attachment and outgrowth of the epicardial cells. Commencing at approximately E10 only *Flrt2* expression is maintained in the fully delaminated epicardium (Muller et al., 2011). The defects in integrity of the epicardial sheet and disturbed organisation of the underlying BM closely resembled that of the *Flrt3*$^{-/-}$ embryos and their failure to maintain cell-cell contacts in the AVE (Maretto et al., 2008).

1.4 Aims of this thesis

Functional activities of *Flrt3* during mouse embryonic development had previously been analysed and reported in the literature (Egea et al., 2008; Haines et al., 2006; Maretto et al., 2008; O'Sullivan et al., 2012; Robinson et al., 2004), *Flrt2* expression patterns and roles in several tissue sites in the developing mouse embryo were also reported (Haines et al., 2006; Lacy et al., 1999; Muller et al., 2011). The closely related family members *Flrt2* and *Flrt3* show several sites of co-expression in the developing mouse embryo (Haines et al., 2006; Maretto et al., 2008). The highly conserved distinct structural features shared between Flrt2 and Flrt3 suggest possible shared functional roles between the two closely related genes. *Flrt2* and *Flrt3* play conserved functional roles in maintaining cell-cell contacts in the epicardium and AVE, respectively (Muller et al., 2011). Ectopic expression of *Flrt2* rescued the BM disorganisation defect in the AVE of the *Flrt3* deficient embryos (Muller et al., 2011).

The aims of this thesis were first to generate *Flrt2*$^{-/-}$*; Flrt3*$^{-/-}$ double mutant embryos in the embryonic lineage (by exploiting the action of Cre recombinase on the *Flrt3*$^{CA/CA}$ allele to delete *Flrt3* in the embryo proper only, not the extra embryonic region), and examine the hypothesis that *Flrt2* and *Flrt3* function cooperatively at sites of their co-expression. The second goal was to generate a *Flrt2 LacZ* reporter/conditional mouse strain, using the EUCOMM/KOMP resource, to further analyse Flrt2 expression patterns and function in the developing mouse embryo.

Chapter 2

Materials and methods

2.1 Materials

All chemicals and reagents were obtained from Sigma-Aldrich unless otherwise stated.

2.1.1 Buffers and solutions

4 % Paraformaldehyde (*PFA)*

4% (w/v) PFA in Phosphate Buffered Saline (PBS).

Crude DNA lysis buffer

10 mM Tris pH 8.5, 50 mM KCl, 1.5 mM $MgCl_2$, 0.45 % NP-40, 0.45 % Tween-20.

Phosphate Buffered Saline (PBS)

137 mM NaCl, 4.3 mM $Na_2HPO_4.7H_2O$, 2.7 mM KCl, 1.4 mM KH_2PO_4, pH 7.3. Alternatively 1 PBS tablet (P4417 – 100 TAB) was dissolved in 200 ml water.

Tris-acetate-EDTA (TAE) buffer

2 M Tris acetate, 100 mM Na, EDTA

X-gal buffer

5 mM EGTA, 2 mM MgCl, 0.04 % NP-40, 0.01 % deoxycholate acid in PBS, pH 7.9.

X-gal fix

1 % formaldehyde, 0.2 % gluteraldehyde in X-gal buffer.

X-gal stain

5 mM K_3Fe, 5 mM K_4Fe, 0.5 % X-gal substrate in X-gal buffer.

2.2 Genomic DNA isolation from mouse ear biopsy/embryonic tissues

Tail tips (from embryos) or ear biopsy samples (from 21 day old (P21) mice) were used for genotyping and identification purposes. Each sample was digested in 100 µl crude DNA lysis buffer containing 500 µg/ml Proteinase K (115 852 001; Roche). Samples were incubated overnight at 55˚C. To heat inactivate the Proteinase K samples were boiled at 95˚C for 10 minutes. 0.5 -1 µl DNA was used for the PCR reaction.

2.3 Polymerase Chain Reaction (PCR)

Standard PCR reactions were performed on BIO-RAD T100 Thermal Cycler Systems. Total reaction volume of 15 µl containing 1 µl of each primer pair or trio (final concentration of 10 mM), 2.5 mM of $MgCl_2$ 2.5 mM and PCR ReddyMix™ mastermix (Thermo Scientific; AB-0575/LD). Thermal cycling conditions varied depending on primers used (**Table 2.1**). Typical PCR conditions used as follows: denaturing at 95˚C for 5 minutes, 25-36 cycles of [denaturing at 95˚C for 30 seconds, annealing at 55-68˚C for 1 minute and extension at 72˚C 1 minute], final elongation at 72˚C for 10 minutes then chilling at 4˚C until further use.

Table 2.1 Primers for standard genotyping

Primer name	Locus	Sequence (5' – 3')``	Temp ˚C (Time)	Cycle no.
F2st KO-	mFlrt2/Flrt2 excised	CTG CCA CAT CCC CAA CAA CAT	64 (1 min)	36
F2st KO-		TCA ACA GCG AAG TGG TTA ATC		
Hyg-		TTT GAA TGG AAG GAT TGG AGC		
F2st KO-		CAG CGT GTC ACT TGC ACT TAC	64 (30	36
JER30	mFlrt3 Conditional	GAT ATT TGC CAA AGG AGA CAG	62 (1 min)	38
JEF38		CTG GGT TCA TTG CTG TCT ACC		
JEF61		AGA GAG CAG AAT GCC GTG		
SIX-A	mFlrt3 Excised	GCA TAA CCA GTG AAA CAG CAT	55 (30 sec)	35
SIX-B		GGA CAT GTT CAG GGA TCG		
WY070	mFlrt2 EUCOMM	CCT TTT ATG GTA ATC GTG CGA	55 (30 sec)	35
WY071		CCA CAA CGG GTT CTT CTG TT		
WY079		CTA AAG GGG AAA CCC GAG TC	58 (30 sec)	35
WY081		TGT TTT GGA TGG CAC TCT GA		
WY220		CCC CCT TTA TTG CGT ATT CTC		

2.4 Gel electrophoresis

PCR products were visualised and separated using gel electrophoresis. DNA fragments were resolved on 3 % agarose gels containing 0.5 ug/ml ethidium bromide in TAE buffer. DNA fragments were visualised using the Gel Logic 200 Imaging System. Images were captured using Kodak MI software.

2.5 Histology techniques

2.5.1 Embryo harvesting and processing for paraffin sectioning

Female mice were checked for vaginal plugs with day of plug detection being embryo day 0.5 (E0.5) and embryos harvested at different stages thereafter. Mice were culled under Schedule 1 according to the Home Office regulations. Uterine horns were removed and embryos were dissected in ice-cold PBS, fixed overnight in 4 % PFA at 4°C, then subsequently dehydrated through a graded ethanol series to 100 % ethanol. Dehydrated embryos were cleared in Histo-Clear® (National Diagnostics) and embedded in 100 % paraffin wax using a Leica EG1160 embedding centre. Sections were cut using a Leica RM2125 RT rotatory microtome and mounted on positively charged SuperFrost® Plus Microscope Slides (VWR International).

2.5.2 Hematoxylin and Eosin staining

Air-dried paraffin sections were rehydrated using a standard rehydration protocol and equilibrated in Milli-Q water for 2 minutes before being placed in Vector® Hematoxylin Gills Formula (H-3401; VectorLabs) for 4 minutes. Slides were gently rinsed with Milli-Q water and placed in Scott's water (2 % (w/v) $MgSO_4$, 0.2 % (w/v) $NaHCO_3$ in Milli-Q water) to ensure the right intensity of blueness then washed with Milli-Q water for 2 minutes. Eosin was used as a

counterstain and slides were stained for up to 1 minute depending on the tissue. After counterstaining, slides were immediately rinsed twice with 95 % ethanol and once with 100 % ethanol and left to air dry at room temperature overnight. Slides were mounted using Cytoseal™ Mounting Medium (8310-16; Thermo Scientific) and photographed using a LEICA DC500 camera system fitted to a LEICA CTR6000 microscope. Images were visualised using the Leica Application Suite software.

2.5.3 X-gal staining

Embryos were dissected in ice-cold PBS and fixed with X-gal fix for 30 minutes to 1 hour depending on the stage of development. The embryos were washed with X-gal buffer 3 times for 10 minutes before staining with X-gal stain at 37˚C overnight. Embryos were washed 3 times with X-gal buffer the following day before fixing in 4 % PFA for 2 hours at 4˚C. The embryos were then washed with X-gal buffer 3 times for 10 minutes and stored in PBS until further use. Selected embryos were processed for sectioning as described in section 2.5.1. Paraffin sections were de-waxed and rehydrated by a standard rehydration protocol before staining with Nuclear Fast Red (Vector Laboratories) for 4 minutes. Slides were allowed to air-dry at room temperature overnight before being mounted as described in section 2.5.2. Selected embryos were taken for photography after being submerged in a graded glycerol series up to 80 %, and images were taken as described in section 2.5.2,

Chapter 3

Generation of *Flrt2* and *Flrt3* double mutant embryos

3.1 Introduction

The Fibronectin Leucine-rich Repeat Transmembrane (Flrt) proteins contain ten leucine-rich repeats, a type III fibronectin domain, followed by the transmembrane region, and a short cytoblasmic tail. The three members of the Flrt family (Flrt1-3) are closely related, sharing the same structural components and have 45% amino acid sequence identity (Lacy et al., 1999). Experiments in this laboratory showed that all three members were expressed broadly across the mouse embryo (Maretto et al., 2008) and embryos lacking *Flrt3* die by embryonic day E10.5 due to defects in ventral closure, headfold fusion and definitive endoderm migration (Maretto et al., 2008). However, embryos homozygous for the *Flrt3* null allele were rescued and developed normally if they contained a wild type copy of the *Flrt3* allele in the extra embryonic tissues, suggesting that that *Flrt3* is needed for the normal development of the extra embryonic tissues but not the embryo itself (Egea et al., 2008). In contrast, the majority of *Flrt2*$^{-/-}$ embryos die between E11.5 and E12.5 due to cardiac insufficiency (Muller et al., 2011).

Flrt2 and *Flrt3* were reported to have several sites of co-expression in the mouse embryo including the heart mesoderm and the pro-epicardial organ (PEO) and at E10.5, *Flrt3* was down regulated while *Flrt2* levels were maintained in the epicardium (outer layer of the heart tissue) (Muller et al,, 2011). The defects in the integrity of the basement membrane of the epicardium described in the *Flrt2*$^{-/-}$ embryos resembled those described in the anterior visceral endoderm (AVE) in mice deficient in *Flrt3* (Muller et al., 2011).

Flrt2 and Flrt3 share similar functions such as mediating homotypic interactions and drive cell sorting behaviour in Xenopus (Karaulanov et al., 2006) and it has also been reported that both genes were functionally

interchangeable and shared similar functional activities *in vivo* (Muller et al., 2011). Interestingly, ectopic *Flrt2* expression can rescue the gastrulation defect in the AVE (Muller et al., 2011). To further understand the unique and possibly shared functional roles of Flrt2 and Flrt3 proteins, study of embryos deficient for both *Flrt2* and *Flrt3* would be extremely beneficial.

The aim of this chapter was to generate *Flrt2* and *Flrt3* double mutant embryos (*Flrt2*$^{-/-}$*; Flrt3*$^{-/-}$) and determine if any differences exist in the morphology and functionality, to expand our existing understanding of functional redundancy between these closely related genes.

3.2 Results

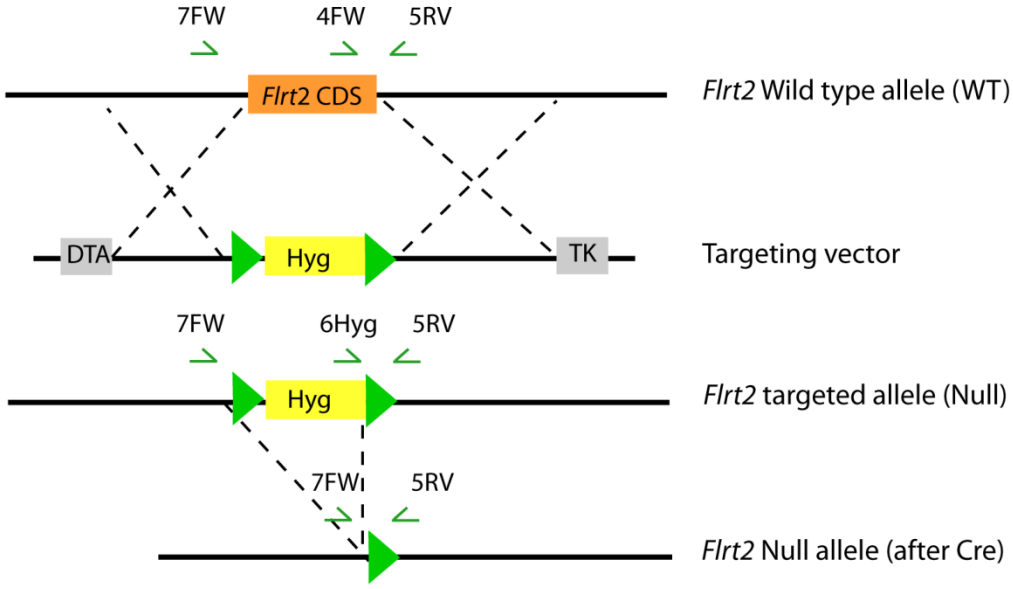
3.2.1 Breeding strategies to generate *Flrt2* and *Flrt3* double mutant embryos

To generate embryos deficient for both *Flrt2* and *Flrt3*, a complicated and time consuming breeding strategy was employed using strains of mice currently available in the laboratory. Firstly, a *Flrt2*$^{+/-}$ strain was previously generated (using gene targeting strategies) whereby the single coding exon (exon 2) was replaced with a hygromycin resistance cassette (Hyg) flanked by two LoxP sites (**Fig 3.1A**). In addition to this, a *Flrt3* conditional allele (CA, kindly donated by Dr. Joaquim Egea, Spain) was generated by inserting two LoxP sites either side of the *Flrt3* coding exon (**Fig 3.1B**). In both instances, the presence of a Cre recombinase will excise the region between the LoxP sites. Both alleles were used to generate male studs and females that carry a combination of the two alleles.

3.2.1.1 Generating *Flrt2*$^{+/-}$; *Flrt3*$^{CA/CA}$ female mice

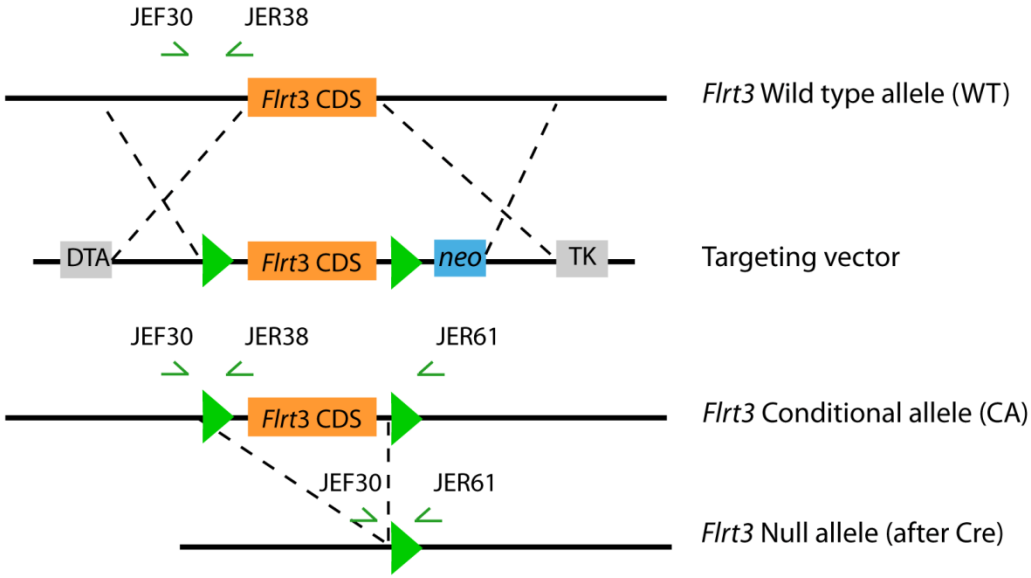
Male mice heterozygous for the *Flrt3* conditional allele (*Flrt3*$^{CA/+}$) were back-crossed to C57BL/6N female mice. After nine weeks when adult mice were sexually mature, the resulting *Flrt3*$^{CA/+}$ offspring were inter-crossed to establish a homozygous colony for the *Flrt3* conditional allele (*Flrt3*$^{CA/CA}$, **Fig 3.2**). The conditional allele with the two LoxP sites flanking the *Flrt3* coding exon was detected by primers (JEF30 and JER38, **Fig 3.2**) that amplified the region on either sides of the LoxP site 5' of the *Flrt3* coding sequence. The total time taken to produce the *Flrt3*$^{CA/CA}$ mice was 20 weeks.

A



Primers:
Wild type: 4FW+5RV 419bp
Targeted allele: 6Hyg+5RV 500bp
Null allele (Cre excised): 7FW+5RV 192bp

B



Primers:
Wild type: JEF30+JER38 399bp
Conditional allele: JEF30+JER38 548bp
Null allele : JEF30+JEF61 610bp

Figure 3.1 Schematic diagram of the targeting strategy used to create the *Flrt2* and *Flrt3* conditional alleles. (A) The *Flrt2* coding sequence (orange rectangle) was replaced with a hygromycin resistance cassette (Hyg, yellow box), which is flanked by two LoxP sites (green triangles), effectively generating a *Flrt2* null allele. In addition, crossing mice carrying the Hyg cassette to Cre recombinase carrier mice will excise the hygromycin resistance cassette, generating a *Flrt2* null allele as well. (B) Two LoxP sites were knocked in 5' and 3' of *Flrt3* coding sequence (orange rectangle) and a neomycin resistance (Neo) cassette (blue box) was used for successful selection. The resulting *Flrt3* conditional allele can produce a null allele by Cre recombinase deletion. Viral thymidine kinase (TK) and Diphtheria toxin A (DTA) negative selection cassettes (grey boxes) were cloned into the targeting construct outside of the homology arms to improve the efficiency of cells that had undergone homologous recombination.

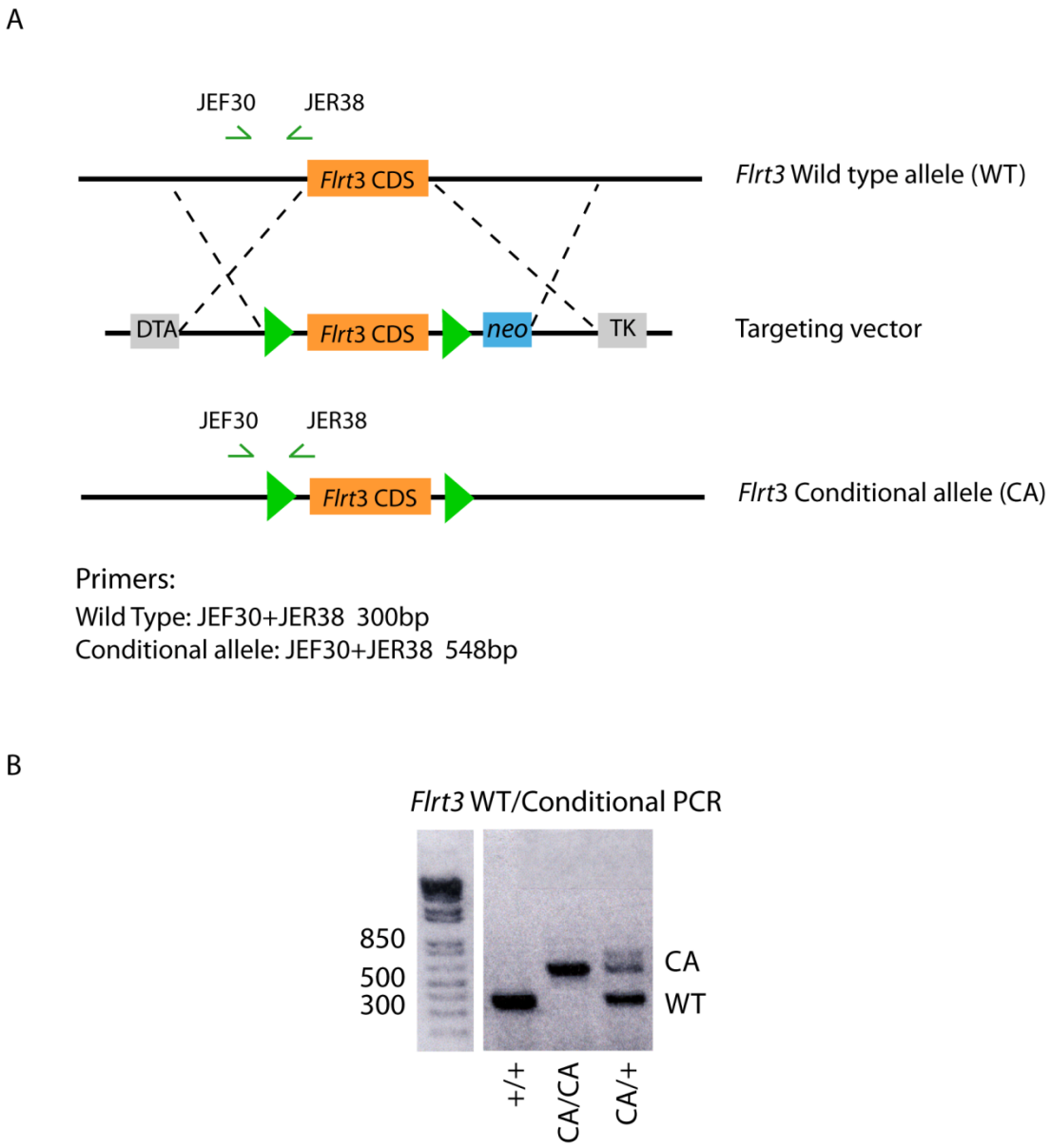


Figure 3.2 Generation of *Flrt3*$^{CA/CA}$ mice. (A) A targeting vector containing the *Flrt3* coding sequence (CDS, orange boxes) flanked by two LoxP sites replaced the wild type coding sequence. Viral thymidine kinase (TK) and Diphtheria toxin A (DTA) negative selection cassettes (grey boxes) were cloned into the targeting construct outside of the homology arms to improve the efficiency of cells that had undergone homologous recombination. (B) Representative pictures showing PCR genotyping results of progeny from *Flrt3*$^{CA/+}$ and *Flrt3*$^{CA/CA}$ intercrosses. The primers (green arrows) amplified 300bp and 548bp products representing the wild type (WT) and conditional allele (CA) respectively.

The resulting *Flrt3*$^{CA/CA}$ mice were then crossed to *Flrt2*$^{+/-}$ mice (as described in section 3.1.1) to create *Flrt2*$^{+/-}$*; Flrt3*$^{CA/+}$ mice. However, as mice homozygous for the *Flrt3* conditional allele were required, *Flrt2*$^{+/-}$*; Flrt3*$^{CA/+}$ mice were intercrossed to finally generate *Flrt2*$^{+/-}$; *Flrt3*$^{CA/CA}$ mice. The targeted *Flrt2* allele where the coding sequence was replaced with a hygromycin selection cassette was differentiated from the wild type allele by a combination of primers that amplified across the wild type allele (4FW and 5RV, **Fig 3.3**) and primers that amplified across the hygromycin resistance cassette (6Hyg and 5RV, **Fig 3.3**).

3.2.1.2 Generating *Flrt2*$^{+/-}$*; Flrt3*$^{+/-}$*; Sox2 Cre* transgene mice

The actions of Cre recombinase were exploited to excise the *Flrt3* CDS in the conditional allele. To generate *Flrt2*$^{+/-}$; *Flrt3*$^{+/-}$ male mice in combination with the *Sox2 Cre* transgene, *Flrt2*$^{+/-}$ male mice were crossed to female mice heterozygous for the *Sox2 Cre* transgene (*Sox2 Cre Tg*$^{+/-}$). The Cre recombinase expressed under the *Sox2* promoter was expressed in the oocytes of the female parent and thus Cre recombinase was expressed in the whole embryo (Hayashi et al,, 2003). Offspring that were heterozygous for the *Flrt2* null allele and expressed the *Sox2 Cre* transgene (*Flrt2*$^{+/-}$; *Sox2 Cre Tg*$^{+/-}$) were collected. Due to the presence of the Sox2 Cre recombinase, the hygromycin selection cassette in the targeted *Flrt2* allele was excised to produce an additional *Flrt2* null allele. The targeted *Flrt2* hygromycin null allele was distinguished from the *Flrt2* null allele (after excision by Sox2 Cre recombinase) by a set of primers that amplified across the hygromycin resistance cassette (6Hyg and 5RV, **Fig 3.4**) and also primers that amplified from either side of the

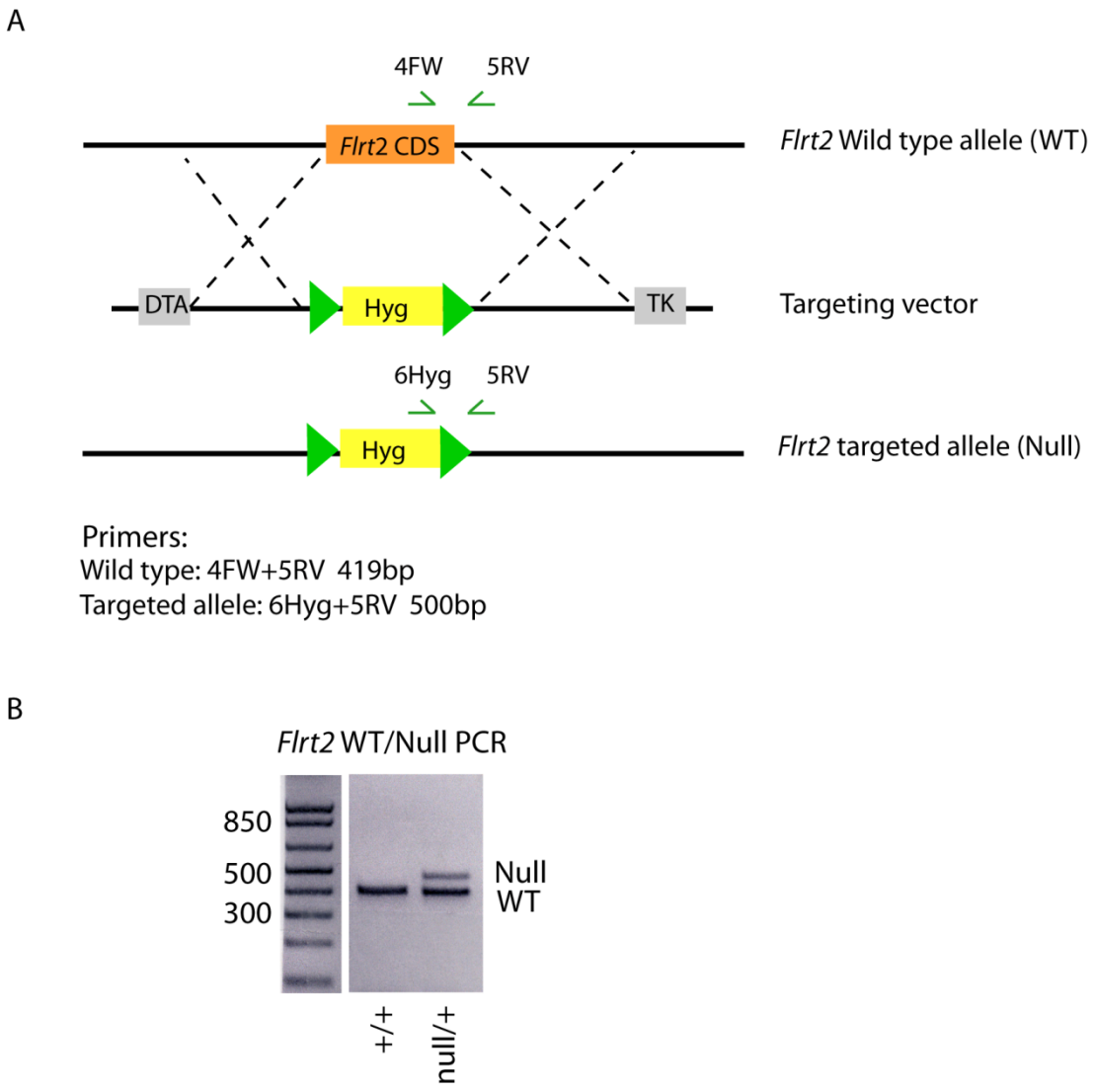


Figure 3.3 Schematic and genotyping for *Flrt2*$^{+/-}$ mice. (A) Targeting vector containing a hygromycin selection cassette (Hyg) replaced the wild type *Flrt2* coding sequence (CDS, orange boxes). Viral thymidine kinase (TK) and Diphtheria toxin A (DTA) negative selection cassettes (grey boxes) were cloned into the targeting construct outside of the homology arms to improve the efficiency of cells that had undergone homologous recombination. (B) Representative picture showing PCR genotyping of progeny from *Flrt2*$^{+/-}$ mice crossed to C57BL6/J mice. The primers (green arrows) amplified 419bp and 500bp products, representing the WT and *Flrt2* null allele respectively.

LoxP sites that flank the hygromycin resistance cassette (7FW and 5RV, **Fig 3.4**).

Flrt2$^{+/-}$; *Sox2 Cre Tg*$^{+/-}$ male mice were then crossed to *Flrt3*$^{CA/CA}$ female mice. As shown in Fig 3.5A, the *Flrt3* CDS was excised by the Sox2 Cre recombinase to produce a *Flrt3* null allele and male offspring were selected for carrying both the *Flrt2* null and *Flrt3* null alleles and which also expressed the *Sox2 Cre* transgene (*Flrt2*$^{+/-}$; *Flrt3*$^{+/-}$; *Sox2 Cre Tg*$^{+/-}$). The *Flrt3* conditional allele was detected by a set of primers flanking either side of the LoxP site 5' of the *Flrt3* CDS (JEF30 and JER38, **Fig 3.5**), and the Sox2 Cre recombined *Flrt3* null allele was detected by another set of primers (JEF30 and JER61, **Fig 3.5**).

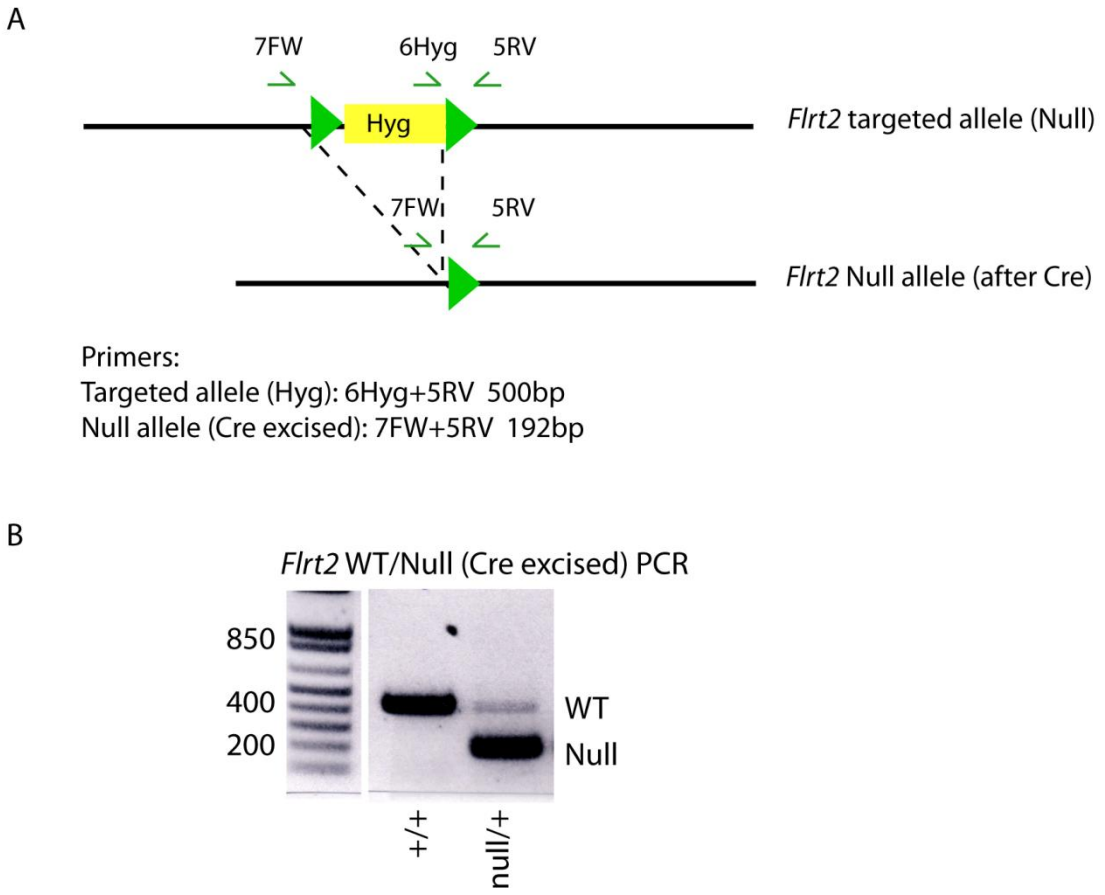


Figure 3.4 Generation of *Flrt2*$^{+/-}$; *Sox2 Cre Tg*$^{+/-}$ mice. (A) The hygromycin resistance cassette (Hyg, yellow box) was excised in the presence of Sox2 Cre recombinase as it is flanked by two LoxP sites (green triangles). The resulting *Flrt2* (Cre excised) allele is also a null. (B) Representative image showing the PCR genotyping of progeny from *Flrt2*$^{+/-}$ male mice crossed to female mice heterozygous for the *Sox2 Cre* transgene (*Sox2 Cre Tg*$^{+/-}$). The primers (green arrows) amplified 419bp and 192bp products representing WT and *Sox2 Cre* recombined alleles respectively.

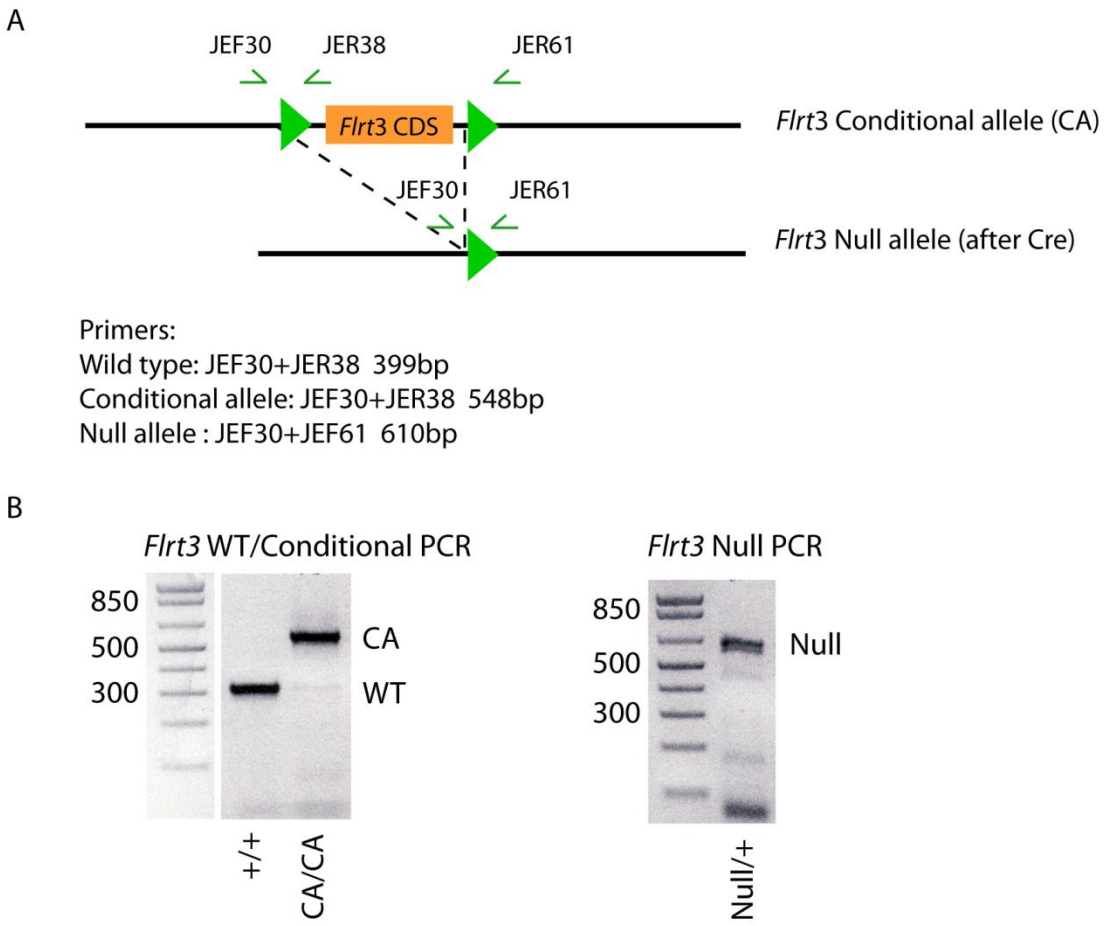


Figure 3.5 Generation of *Flrt2*$^{+/-}$; *Flrt3*$^{+/-}$; *Sox2 Cre Tg*$^{+/-}$ mice. (A) The *Flrt3* CDS (orange rectangle) flanked by two LoxP sites (green triangles) was deleted by Sox2 Cre recombination which generated a *Flrt3* null allele. (B) Representative image showing PCR gentoping of progeny from homozygous *Flrt3*$^{CA/CA}$ mice crossed to *Flrt2*$^{+/-}$; *Sox2 Cre Tg*$^{+/-}$ mice. The *Flrt3* CDS was excised in the presence of Sox2 Cre recombinase producing a heterozygous null allele (*Flrt3*$^{+/-}$). The primers (green arrows) amplified 300bp and 548bp products, representing the WT and conditional allele respectively. A 610bp product was formed after Sox2 Cre recombination.

3.2.2 Generation of *Flrt2*$^{-/-}$; *Flrt3*$^{-/-}$ double mutant embryos

To investigate the function of Flrt2 in the absence of Flrt3 and vice versa, mice carrying the *Flrt3* conditional allele was used in combination with the *Sox2 Cre* transgene to selectively knockout *Flrt3* from the embryos proper (Hayashi et al., 2002). Initially, female mice homozygous for the *Flrt3* conditional allele (*Flrt3*$^{CA/CA}$) were crossed to *Flrt2*$^{+/-}$ male mice to establish a colony of *Flrt2*$^{+/-}$; *Flrt3*$^{CA/CA}$, as explained in section 3.2.1.1. The *Flrt2*$^{+/-}$; *Flrt3*$^{CA/CA}$ female mice were then crossed to *Flrt2*$^{+/-}$; *Flrt3*$^{+/-}$; *Sox2 Cre Tg*$^{+/-}$ male mice (as described in section 3.2.1.2). Crossing *Flrt2*$^{+/-}$;*Flrt3*$^{CA/CA}$ female mice to *Flrt2*$^{+/-}$; *Flrt3*$^{+/-}$; *Sox2 Cre Tg*$^{+/-}$ male mice produced offspring of a range of genotypes, some of which were *Flrt2*$^{-/-}$ or *Flrt3*$^{-/-}$ and also the required *Flrt2*$^{-/-}$; *Flrt3*$^{-/-}$ (**Fig 3.6).** The expected Mendelian ratios of the *Flrt2*$^{-/-}$ and *Flrt3*$^{-/-}$ embryos were 18.75% each, however, due to the complicated nature of inheritance, only an expected 1 in 16 (or 6.25%) of the offspring was of the *Flrt2*$^{-/-}$; *Flrt3*$^{-/-}$ genotype (**Fig 3.7**). A Punnet square diagram, as shown in **Fig 3.8,** shows all the different possible genotypes that could be obtained from this mating strategy.

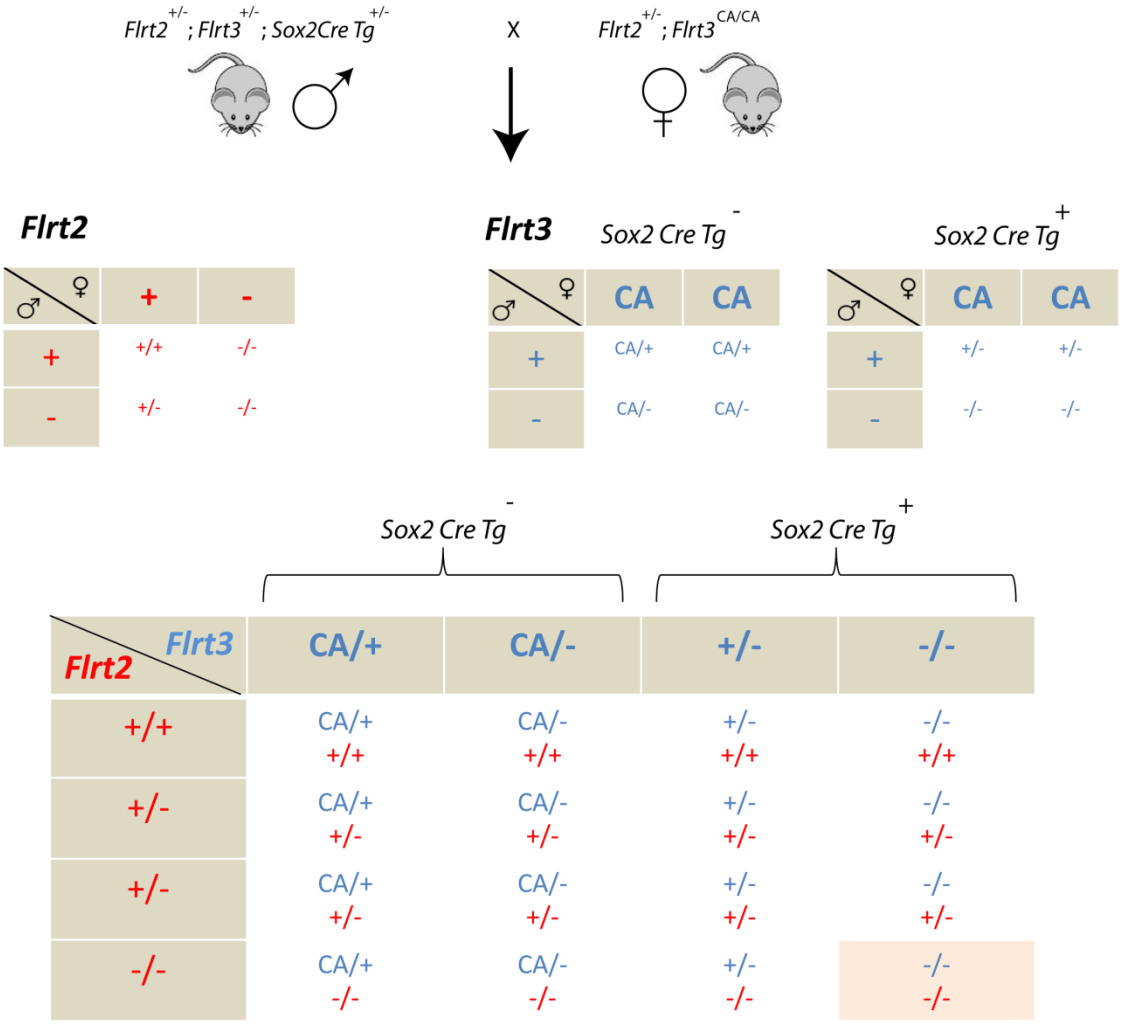


Figure 3.6 Schematic diagram for the generation of *Flrt2*$^{-/-}$; *Flrt3*$^{-/-}$ mice. *Flrt2*$^{+/-}$; *Flrt3*$^{+/-}$; *Sox2 Cre Tg*$^{+/-}$ male mice were crossed to *Flrt2*$^{+/-}$; *Flrt3*$^{CA/CA}$ female mice. Offspring was expected to inherit different combinations of *Flrt2* (red) and *Flrt3* (blue) alleles from each parent. 1 in 16 of those combinations was expected to receive a null allele for both *Flrt2* and *Flrt3* (pink shaded).

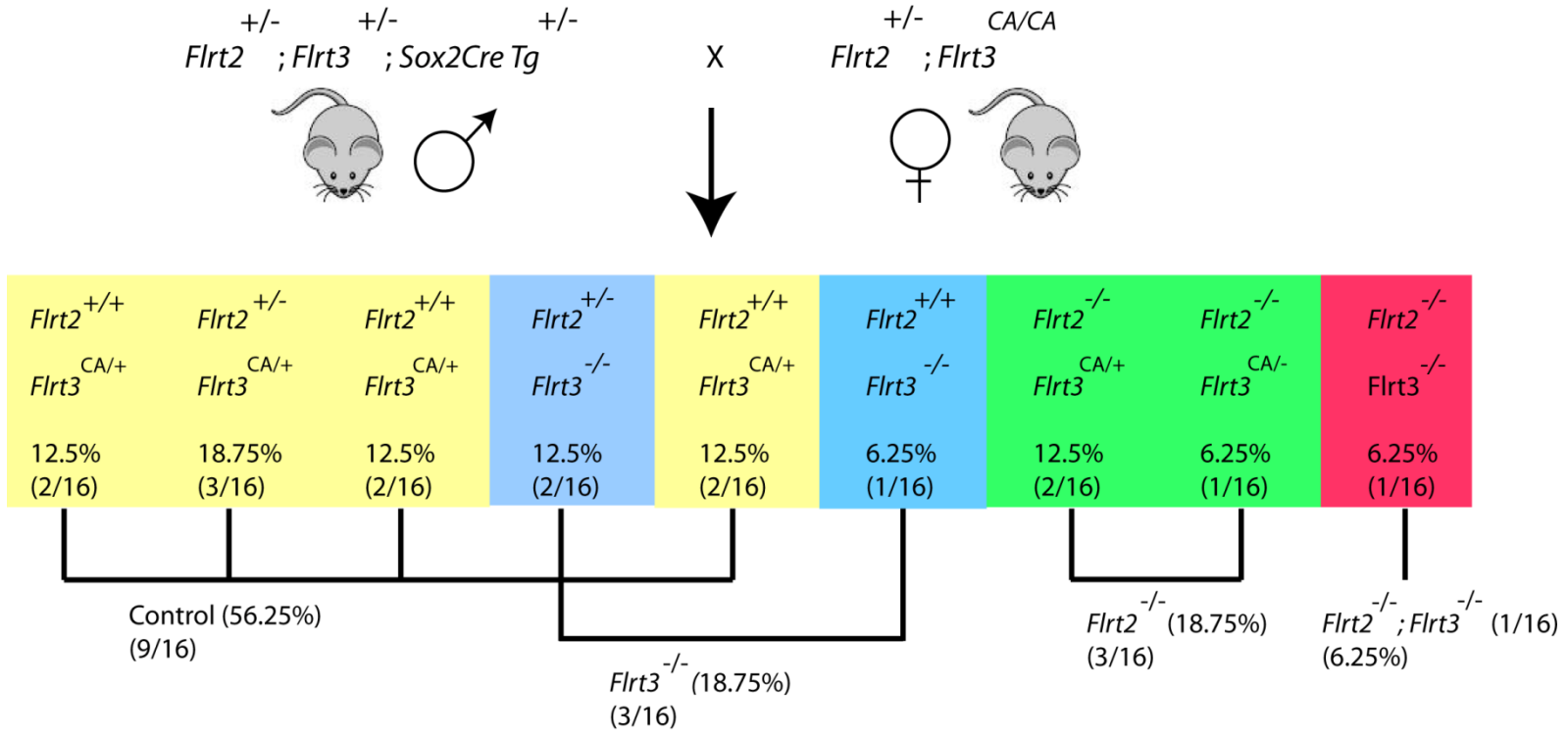


Figure 3.7 Schematic representation of the breeding strategy for generating *Flrt2*$^{-/-}$; *Flrt3*$^{-/-}$ embryos. *Flrt2*$^{+/-}$; *Flrt3*$^{+/-}$; *Sox2 Cre Tg*$^{+/-}$ male mice were crossed with *Flrt2*$^{+/-}$; *Flrt3*$^{CA/CA}$ female mice to generate the various genotypes as shown. The cross generated wild type controls (yellow boxes), *Flrt2*$^{-/-}$ (green box), *Flrt3*$^{-/-}$ (blue boxes) and *Flrt2*$^{-/-}$; *Flrt3*$^{-/-}$ double mutant embryos (red box). Expected mendelian ratios are also shown.

Flrt2$^{+/-}$; Flrt3$^{+/-}$; Sox2 Cre Tg$^{+/-}$ **X** ***Flrt2$^{+/-}$; Flrt3$^{+/-}$; Sox2 Cre Tg$^{-/-}$***



	Flrt2^{-}; *Flrt3*^{CA}; Tg Cre^{-}	*Flrt2*$^{-}$; *Flrt3*^{CA}; Tg Cre^{-}	*Flrt2*$^{-}$; *Flrt3*^{CA}; Tg Cre^{-}	*Flrt2*$^{-}$; *Flrt3*^{CA}; Tg Cre^{-}	*Flrt2*$^{+}$; *Flrt3*^{CA}; Tg Cre^{-}	*Flrt2*$^{+}$; *Flrt3*^{CA}; Tg Cre^{-}	*Flrt2*$^{+}$; *Flrt3*^{CA}; Tg Cre^{-}	*Flrt2*$^{+}$; *Flrt3*^{CA}; Tg Cre^{-}
Flrt2^{-}; *Flrt3*$^{-}$; Tg Cre^{+}	*Flrt2*$^{-/-}$; *Flrt3*$^{-/-}$; Tg Cre^{+}	*Flrt2*$^{-/-}$; *Flrt3-/-*; Tg Cre +	*Flrt2*$^{-/-}$; *Flrt3*$^{-/-}$; Tg Cre^{+}	*Flrt2*$^{-/-}$; *Flrt3*$^{-/-}$; Tg Cre^{+}	*Flrt2*$^{+/-}$; *Flrt3*$^{-/-}$; Tg Cre^{+}	*Flrt2*$^{+/-}$; *Flrt3*$^{-/-}$; Tg Cre^{+}	*Flrt2*$^{+/-}$; *Flrt3*$^{-/-}$; Tg Cre^{+}	*Flrt2*$^{+/-}$; *Flrt3*$^{-/-}$; Tg Cre^{+}
Flrt2^{-}; *Flrt3*$^{-}$; Tg Cre^{-}	*Flrt2*$^{-/-}$; *Flrt3* $^{CA/-}$; Tg Cre^{-}	*Flrt2*$^{-/-}$; *Flrt3* CA/-; Tg Cre -	*Flrt2*$^{-/-}$; *Flrt3*$^{CA/-}$; Tg Cre^{-}	*Flrt2*$^{-/-}$; *Flrt3*$^{CA/-}$; Tg Cre^{-}	*Flrt2*$^{+/-}$; *Flrt3*$^{CA/-}$; Tg Cre^{-}	*Flrt2*$^{+/-}$; *Flrt3*$^{CA/-}$; Tg Cre^{-}	*Flrt2*$^{+/-}$; *Flrt3*$^{CA/-}$; Tg Cre^{-}	*Flrt2*$^{+/-}$; *Flrt3*$^{CA/-}$; Tg Cre^{-}
Flrt2^{-}; *Flrt3*$^{+}$; Tg Cre^{+}	*Flrt2*$^{-/-}$; *Flrt3* $^{-/+}$; Tg Cre^{+}	*Flrt2*$^{-/-}$; *Flrt3*$^{-/+}$; Tg Cre^{+}	*Flrt2*$^{-/-}$; *Flrt3*$^{-/+}$; Tg Cre^{+}	*Flrt2*$^{-/-}$; *Flrt3*$^{-/+}$; Tg Cre^{+}	*Flrt2*$^{+/-}$; *Flrt3*$^{-/+}$; Tg Cre^{+}	*Flrt2*$^{+/-}$; *Flrt3-*$^{/+}$; Tg Cre^{+}	*Flrt2*$^{+/-}$; *Flrt3*$^{-/+}$; Tg Cre^{+}	*Flrt2*$^{+/-}$; *Flrt3*$^{-/+}$; Tg Cre^{+}
Flrt2^{-}; *Flrt3*$^{+}$; Tg Cre^{-}	*Flrt2*$^{-/-}$; *Flrt3*$^{CA/+}$; Tg Cre^{-}	*Flrt2*$^{-/-}$; *Flrt3*$^{CA/+}$; Tg Cre -	*Flrt2*$^{-/-}$; *Flrt3*$^{CA/+}$; Tg Cre^{-}	*Flrt2*$^{-/-}$; *Flrt3*$^{CA/+}$; Tg Cre -	*Flrt2*$^{+/-}$; *Flrt3*$^{CA/+}$; Tg Cre^{-}	*Flrt2*$^{+/-}$; *Flrt3*$^{CA/+}$; Tg Cre^{-}	*Flrt2*$^{+/-}$; *Flrt3*$^{CA/+}$; Tg Cre^{-}	*Flrt2*$^{+/-}$; *Flrt3*$^{CA/-}$; Tg Cre^{-}
Flrt2^{+}; *Flrt3*$^{-}$; Tg Cre^{+}	*Flrt2*$^{-/+}$; *Flrt3*$^{-/-}$; Tg Cre^{+}	*Flrt2*$^{-/+}$; *Flrt3*$^{-/-}$; Tg Cre^{+}	*Flrt2*$^{-/+}$; *Flrt3*$^{-/-}$; Tg Cre^{+}	*Flrt2*$^{-/+}$; *Flrt3*$^{-/-}$; Tg Cre^{+}	*Flrt2*$^{+/+}$; *Flrt3*$^{-/-}$; Tg Cre^{+}	*Flrt2*$^{+/+}$; *Flrt3*$^{-/-}$; Tg Cre^{+}	*Flrt2*$^{+/+}$; *Flrt3*$^{-/-}$; Tg Cre^{+}	*Flrt2*$^{+/+}$; *Flrt3*$^{-/-}$; Tg Cre^{+}
Flrt2^{+}; *Flrt3*$^{-}$; Tg Cre^{-}	*Flrt2*$^{-/+}$; *Flrt3*$^{CA/-}$; Tg Cre^{-}	*Flrt2*$^{-/+}$; *Flrt3*$^{CA/-}$; Tg Cre^{-}	*Flrt2*$^{-/+}$; *Flrt3*$^{CA/-}$; Tg Cre^{-}	*Flrt2*$^{-/+}$; *Flrt3*$^{CA/-}$; Tg Cre^{-}	*Flrt2*$^{+/+}$; *Flrt3*$^{CA/-}$; Tg Cre^{-}	*Flrt2*$^{+/+}$; *Flrt3*$^{CA/-}$; Tg Cre^{-}	*Flrt2*$^{+/+}$; *Flrt3*$^{CA/-}$; Tg Cre^{-}	*Flrt2*$^{+/+}$; *Flrt3*$^{CA/-}$; Tg Cre^{-}
Flrt2^{+}; *Flrt3*$^{+}$; Tg Cre^{+}	*Flrt2*$^{-/+}$; *Flrt3*$^{-/+}$; Tg Cre^{+}	*Flrt2*$^{-/+}$; *Flrt3*$^{-/+}$; Tg Cre^{+}	*Flrt2*$^{-/+}$; *Flrt3*$^{-/+}$; Tg Cre^{+}	*Flrt2*$^{-/+}$; *Flrt3*$^{-/+}$; Tg Cre^{+}	*Flrt2*$^{+/+}$; *Flrt3*$^{-/+}$; Tg Cre^{+}	*Flrt2*$^{+/+}$; *Flrt3*$^{-/+}$; Tg Cre^{+}	*Flrt2*$^{+/+}$; *Flrt3*$^{-/+}$; Tg Cre^{+}	*Flrt2*$^{+/+}$; *Flrt3*$^{-/+}$; Tg Cre^{+}
Flrt2^{+}; *Flrt3*$^{+}$; Tg Cre^{-}	*Flrt2*$^{-/+}$; *Flrt3*$^{CA/+}$; Tg Cre^{-}	*Flrt2*$^{-/+}$; *Flrt3*$^{CA/+}$; Tg Cre^{-}	*Flrt2*$^{-/+}$; *Flrt3*$^{CA/+}$; Tg Cre^{-}	*Flrt2*$^{-/+}$; *Flrt3*$^{CA/+}$; Tg Cre^{-}	*Flrt2*$^{+/+}$; *Flrt3*$^{CA/+}$; Tg Cre^{-}	*Flrt2*$^{+/+}$; *Flrt3*$^{CA/+}$; Tg Cre^{-}	*Flrt2*$^{+/+}$; *Flrt3*$^{CA/+}$; Tg Cre^{-}	*Flrt2*$^{+/+}$; *Flrt3*$^{CA/+}$; Tg Cre^{-}

*Sox2 Cre transgene (Tg Cre +) will be passed on by the father in a rate of 50% as it's carried on one chromosome only. The mother doesn't have the transgene (Tg Cre-).

Figure 3.8 Punnett square with gamete segregation from each parent and all possible genotypes. *Flrt2*$^{-/-}$; *Flrt3*$^{-/-}$ double mutant embryos (red boxes) produced when the father passes on *Flrt3* null allele (*Flrt3*$^{-}$) and the *Flrt3* conditional allele (*Flrt3*^{CA}) passed on by the mother rearranged by Sox2 Cre transgene (passed on by the father only), and both parents pass on their *Flrt2* null alleles (*Flrt2*$^{-}$). Otherwise embryos will be either wild type controls (yellow boxes), *Flrt2*$^{-/-}$ (green boxes) or *Flrt3*$^{-/-}$ (blue boxes).

3.2.3 Recovery of *Flrt2*$^{-/-}$; *Flrt3*$^{-/-}$ embryos at E9.5 and E10.5

Embryos from the animal crossing strategy outlined in section 3.2.2 were initially collected at E10.5 as previous experiments in this laboratory established that embryos lacking *Flrt3* were unable to survive post E10.5 (Maretto et al., 2008). At E10.5 the expected Mendelian ratios for single *Flrt2*$^{-/-}$ and *Flrt3*$^{-/-}$ mutants were obtained (18.8% and 17.5% observed respectively vs. 18.75% expected), however this was not observed with the *Flrt2*$^{-/-}$; *Flrt3*$^{-/-}$ double mutant embryos (3% observed vs. 6.25% expected, Table 3.1). Statistical analysis of the expected vs. observed percentages at E10.5 for *Flrt2*$^{-/-}$; *Flrt3*$^{-/-}$ embryos revealed a chi square value (X^2) of 0.67 with a degree of freedom of three. Since X^2 exceeds the critical value of probability ($p \geq 0.05$), this was statistically significant and the null hypothesis (the observed values of the cross was the same as the theoretical distribution) was rejected. Therefore, embryos were collected at an earlier stage to determine if it was possible to collect the correct Mendelian ratios for all genotypes.

Embryos were collected at E9.5 and the expected Mendelian ratio of *Flrt2*$^{-/-}$; *Flrt3*$^{-/-}$ embryos were recovered (6.8% observed vs. 6.25% expected, as well as the expected ratios of *Flrt2*$^{-/-}$ and *Flrt3*$^{-/-}$ single mutants (19.3% and 18.1% respectively vs. 18.75% expected, Table 3.1).

Table 3.1 Total number of embryos collected in the *Flrt2*$^{-/-}$*; Flrt3*$^{-/-}$ breeding strategy. The table represents the number of embryos collected at E9.5 and E10.5. The percentages of each genotype are shown in brackets

Embryonic stage	Total number of embryos collected	Number of control embryos (%)	Number of *Flrt2*$^{-/-}$ embryos (%)	Number of *Flrt3*$^{-/-}$ embryos (%)	Number of *Flrt*$^{-/--}$ *; Flrt3*$^{-/-}$ embryos (%)
E9.5	176	98 (55.8%)	34 (19.3%)	32 (18.1%)	12 (6.8%)
E10.5	143	87 (60.7%)	27 (18.8%)	25 (17.5%)	4 (3%)

.

3.2.4 Conclusion

Both Flrt2 and Flrt3 are extremely important cell adhesion molecules that are expressed in a number of tissues in the body (Lacy et al., 1999). Experiments in this laboratory have shown that mice deficient in either one of *Flrt2* or *Flrt3* are embryonic lethal due to cardiac insufficiency, and structural defect in the AVE and a fusion failure of the lateral body walls of the embryo respectively (Maretto et al., 2008; Muller et al., 2011). *Flrt2* and *Flrt3* had partial overlapping expression in the developing heart of the mouse embryo (Maretto et al., 2008; Muller et al, 2011). At an early stage during development (E10), *Flrt3* was selectively downregulated and only *Flrt2* expression was maintained in the epicardial layer that invades and surrounds the developing heart (Muller et al., 2011).

Of particular note, ectopic expression of *Flrt2* corrects the abnormal morphology in the AVE of the *Flrt3* deficient embryoid bodies (EBs) *in vitro*, and transgenic embryos lacking one of the two genes (*Flrt2* or *Flrt3*) and ectopically expressing the other were successfully rescued, suggesting that expression of one can compensate for the lack of the other (Muller et al., 2011). This phenomenon of functional redundancy between closely related genes of the same family is common. For example, two closely related genes of the TGF-β family of secreted growth factors, *Smad1* and *Smad5*, are activated by Bone morphogenetic protein (BMP) receptors. The two so-called R-Smads (Smad1+Smad5), function cooperatively to govern BMP signalling (Arnold, 2006). The phenotypic similarity in the defects in ventral closure, heart, vascular system and allantois (Chang et al., 1999; Yang et al., 1999) of the $Smad1^{+/-}$; $Smad5^{+/-}$ double heterozygous embryos, with those lacking either *Smad1* or *Smad5* strongly suggest that they share the same signalling functions. *Flrt2* and

Flrt3 are also closely related family members of the Flrt family of proteins. Therefore, it was of interest to determine what the effects were when neither *Flrt2* nor *Flrt3* was present.

The results of this chapter showed that it was feasible to produce mouse embryos that were deficient in both *Flrt2* and *Flrt3* and as expected, these mice were embryonic lethal at E10.5. The percentage of *Flrt2*$^{-/-}$ embryos collected at E10.5 was of the correct Mendelian ratio (18.8% observed vs. 18.75 expected, Table 3.1), but the percentage of embryos with the *Flrt2*$^{-/-}$*; Flrt3*$^{-/-}$ genotype was not (3% observed vs. 6.25% expected).

The exact cause of embryonic lethality in *Flrt2*$^{-/-}$*; Flrt3*$^{-/-}$ is presently unclear as it was beyond the scope and timeframe of this project. As mentioned previously*, in vivo* ectopic expression of *Flrt2* rescued the disturbance of the basement membrane (BM) of *Flrt3* deficient EBs in the same way the *in vitro* ectopic expression of *Flrt3* restored the epicardial integrity of the *Flrt2*$^{-/-}$ transgenic embryos (Muller et al., 2011), so one possibility is that there is no compensation mechanism present when both *Flrt2* and *Flrt3* were absent.

Flrt3 is perhaps, in one way or another, functioning to maintain the integrity of the epicardial sheet in the *Flrt2*$^{-/-}$ embryos, and when lost the *Flrt2*$^{-/-}$*; Flrt3*$^{-/-}$ embryos fail to develop beyond E10.5. This possibility is supported by the fact that *Flrt3* expression is maintained in the epicardium up until E10. However, expression level of *Flrt3* then goes down dramatically in the epicardium beyond E10. Perhaps this is when the damage to epicardial tissue layer becomes too severe and *Flrt2*$^{-/-}$ embryos die between E11.5 and E12.5 due to cardiac insufficiency (Muller et al., 2011). The results also suggest that up until E9.5 *Flrt2*$^{-/-}$*; Flrt3*$^{-/-}$ can still survive and the effect of losing both *Flrt2* and *Flrt3* together is more severe than losing either of them individually.

In summary, this genetic experiment demonstrates that the *Flrt2*$^{-/-}$; *Flrt3*$^{-/-}$ embryos exhibit a more severe phonotype than the single mutants, potentially due to the fact the two genes are functioning cooperatively in sites of their co-expression, and loss of both has a more severe impact on embryonic development.

Chapter 4

Generation of *Flrt2* reporter and conditional alleles

4.1 Introduction

The International Knockout Mouse Consortium (IKMC) is an international project that aims to generate mutations in virtually every protein coding gene in the mouse genome in a cooperative and concerted worldwide effort (Bradley et al, 2012; Skarnes et al, 2011). The European Conditional Mouse Mutagenesis Program (EUCOMM), Knockout Mouse Project (KOMP), North American Conditional Mouse Mutagenesis Project (NorCOMM), and the Texas A&M Institute for Genomic Medicine (TIGM) were the founding programmes of the IKMC. The EUCOMM/KOMP resource contains an allele design known as “knockout-first”, from which a conditional or a reporter allele can be established following exposure to site-specific recombinase (Bradley et al., 2012; Skarnes et al., 2011)

Embryonic Stem Cells (ESCs) represent an excellent model to study development. ESCs harbouring a conditional allele have proven to be a very useful tool in studying gene function in stem cell self renewal, embryonic development and differentiation (Haupt et al., 2007). The site-specific recombinase Cre has been used to introduce genetic alteration in a variety of ways by site-specific recombination of previously integrated LoxP sites. The LoxP sites are sequences of 34 base pairs that can be recognised by Cre recombinase and any sequence flanked by two LoxP sites can be recombined. This phenomenon can be used in a variety of ways such as deleting a sequence of a gene or a promoter (knockout) or introducing a sequence of DNA, for example, enhancers (knock in) (Haupt et al., 2007). Therefore, it was feasible to generate the *Flrt2* reporter/conditional mouse strain using the EUCOMM/KOMP resource by micro-injection of targeted ESCs into blastocysts to generate germline chimera.

As mentioned previously, *Flrt2* functional activities *in vivo* and expression patterns in mouse embryos have previously been studied (Maretto et al., 2008; Muller et al., 2011) and an insight into the temporal onset of Flrt2 protein expression has been described (Haines et al, 2006; Maretto et al., 2008). However, previous studies described *Flrt2* function by generating a null allele resulting in embryo wide *Flrt2* deletion.

Flrt2 has been shown to be expressed in a range of tissues including the pancreas, skeletal muscle, brain, and heart (Lacy et al, 1999). As shown in numerous occasions, the same protein may have different functions depending on the site of expression. For example, the microsomal triglyceride transfer protein (MTP) is a cellular protein involved in transferring neural lipids between membrane vesicles but its function varies depending on the tissue type (Hussain et al., 2012; Wetterau and Zilversmit, 1984). In the liver, MTP mobilises dietary and endogenous fats into other tissues (Hussain et al., 2012), whereas it protects cholesterol crystal deposition in the heart (Nielsen et al., 2002) and retina (Li et al., 2005). As there is little understanding regarding the function of Flrt2 in different tissue types, it would be of particular interest to determine the effects of tissue specific deletion of *Flrt2* to allow for further dissection of its function.

In addition, current methods for determining sites of Flrt2 expression involve complicated and time consuming protocols such as whole embryo *in situ* hybridisation (WISH) or sectioning and staining tissue for histology. A much simpler and easier system would be to exploit the LacZ system (Kothary et al., 1989). The *LacZ* gene encodes for β-galactosidase, an enzyme that breaks down X-gal (5-bromo-4-chloro-indolyl-β-D-galactopyranoside) resulting in a blue

by product. In this case, by placing *LacZ* downstream of the Flrt2 promoter, blue colour formation would indicate sites of *Flrt2* expression.

No known reporter or conditional allele for *Flrt2* has been generated and analysed previously. The aim of this chapter was to use the EUCOMM/KOMP *Flrt2* targeted allele to generate a *Flrt2 LacZ* reporter and a conditional allele to allow for expression pattern analysis and studying the phenotypic consequences of tissue specific deletion of *Flrt2*.

4.2 Results

4.2.1 Generating *Flrt2* reporter/conditional allele using targeting via ESC technology

ESCs containing the *Flrt2* targeted allele generated by the EUCOMM/KOMP resource were obtained from the Sanger Institute, United Kingdom. The *Flrt2* EUCOMM/KOMP vector contains an internal ribosomal entry site (IRES) derived *LacZ* reporter gene flanked by two FRT site-specific recombination sites (red rectangles, **Fig 4.1**), and two LoxP sites integrated either side of the *Flrt2* coding sequence (green triangles, **Fig 4.1**). The IRES allows for translation initiation in the middle of a messenger RNA (mRNA) sequence without the need for a start codon (Pelletier et al., 1988). The *Flrt2* conditional allele was generated by FLP recombination whereby the FLP recombinase enzyme recognises the FRT sites and excises the sequence between the two FRT sites. Additionally, the *Flrt2* conditional allele can also generate a *Flrt2* null allele by Cre recombination (**Fig 4.1**). Two clones from the EUCOMM/KOMP resource containing the *Flrt2* targeted allele were used to generate germline chimeras by microinjection into C57BL6/J blastocysts (performed by Prof. Elizabeth Robertson, University of Oxford).

4.2.2 PCR confirmation of the *Flrt2* EUCOMM/KOMP targeted allele

Chimeric male mice generated from the *Flrt2* EUCOMM/KOMP targeted cells were crossed to C57BL6/J female mice, and heterozygous male offspring were backcrossed to C57BL6/J female mice to establish a *Flrt2 LacZ* reporter mouse strain (**Fig 4.2A**). As mentioned previously, as *LacZ* is downstream of the *Flrt2* promoter, blue colour formation would indicate sites of *Flrt2* expression (**Fig**

4.2A). The total time taken to generate the *Flrt2 LacZ* reporter strain was 20 weeks.

The *Flrt2* EUCOMM/KOMP targeting vector contains a *LacZ* and neomycin resistance selection cassette upstream of the *Flrt2* coding sequence. The *LacZ* sequence and neomycin selection cassette are flanked by two FRT sites and two LoxP sites lie either side of the *Flrt2* coding sequence (**Fig 4.2A**). The wild type allele was detected by PCR with a combination of primers that amplified across the 5' homology arm and the intron of the *Flrt2* coding sequence (WY220 and WY081, **Fig 4.2**), whereas the *Flrt2* EUCOMM/KOMP targeted allele was detected by a set of primers that amplified within the *LacZ* reporter gene and the intron 5' of *Flrt2* coding sequence (WY220 and WY071, **Fig 4.2**).

4.2.3 Generation of the *Flrt2* conditional mouse strain

Flrt2 LacZ heterozygous mice (*Flrt2*$^{m/+}$) were crossed to *Rosa 26-FLP* homozygous mice (*Rosa 26*$^{FLP/FLP}$), where the FLP recombinase was driven under control of the ubiquitously expressed Rosa 26 promoter, to generate the *Flrt2* conditional allele mouse strain. In the presence of FLP recombinase the *LacZ* reporter and the neomycin resistance selection cassette was excised to generate the *Flrt2* conditional allele (**Fig 4.3**). The total time taken to generate the *Flrt2* conditional mice (*Flrt2*$^{CA/CA}$) was 20 weeks and these mice were viable.

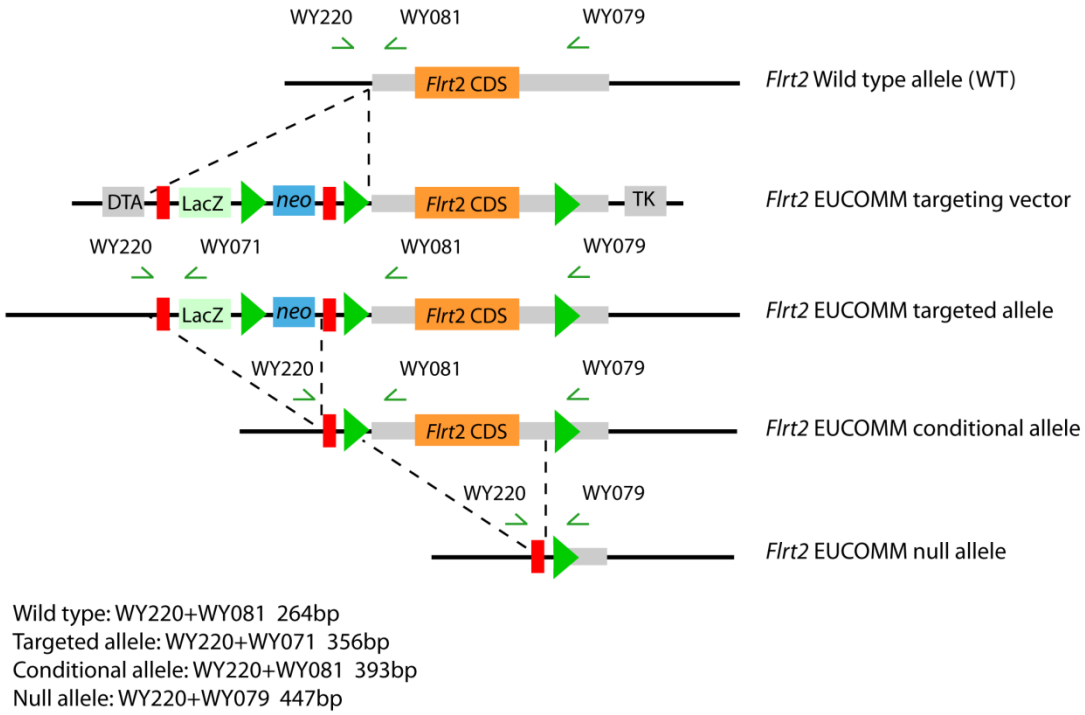


Figure 4.1 Targeting strategy for generating a *Flrt2* conditional allele using the EUCOMM/KOMP vector The targeting vector with the LacZ trapping cassette (light green box) and a promoter-driven neomycin resistance cassette (neo, blue box) flanked by two LoxP sites (green triangles) was inserted upstream of the *Flrt2* coding exon (orange box). The LacZ and neo cassettes were flanked by two FRT sites (red boxes). FLP recombinase excised the region between the FRT sites to generate a *Flrt2* conditional allele. Cre recombinase excised the entire region between the LoxP sites resulting in a *Flrt2* null allele. TK and DTA negative selection cassettes (grey boxes) were cloned into the targeting construct outside of the homology arms to improve the efficiency of cells that had undergone homologous recombination.

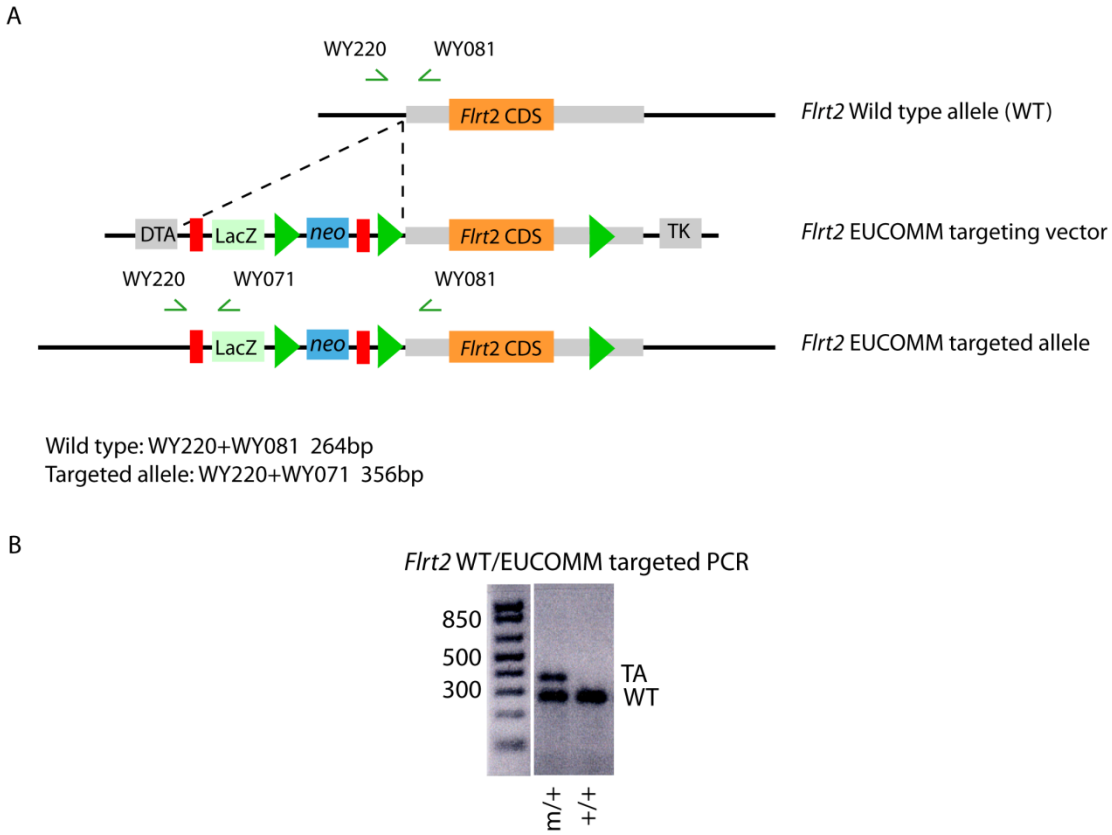


Figure 4.2 Schematic diagram showing the *Flrt2* EUCOMM/KOMP targeted allele and PCR verification (A) The *Flrt2* EUCOMM/KOMP targeted allele contains a *LacZ* reporter sequence (green boxes) and neomycin resistance selection cassette (blue boxes) upstream of the *Flrt2* CDS (orange boxes) on the 5' targeting arm (grey). (B) PCR genotyping of a progeny from heterozygous *Flrt2 LacZ* targeted offspring backcrossed to C57BL6/J female mice. The primers (green arrows) amplified 264 bp and 356bp products, representing the WT and targeted allele respectively.

Mice heterozygous for the *Flrt2* conditional allele (*Flrt2*$^{CA/+}$) were then crossed to *Sox2 Cre Tg*$^{+/-}$ mice to examine the fidelity of the *Flrt2* conditional allele. Successful deletion of the *Flrt2* CDS and generation of *Flrt2*$^{+/-}$ mice indicated that the conditional allele was functioning properly and the sequence between the LoxP sites was excised. The total time taken to generate *Flrt2*$^{+/-}$ mice from the EUCOMM/KOMP allele was 20 weeks.

Flrt2$^{+/-}$ mice generated from the EUCOMM/KOMP allele were intercrossed to determine if this allele generates a recessive embryonic lethal phenotype at E11.5-E12.5 as previously described in our lab (Muller et al,, 2011). As expected, *Flrt2*$^{+/-}$ mice were successfully generated and no *Flrt2*$^{-/-}$ mice were obtained, suggesting that the EUCOMM/KOMP allele was functioning properly and the *Flrt2* CDS was excised. However, the number of mice collected was not sufficient to be analysed statistically (24 embryos of which 15 were wild type and 9 were heterzygoute mutants), and further intercrosses are currently ongoing.

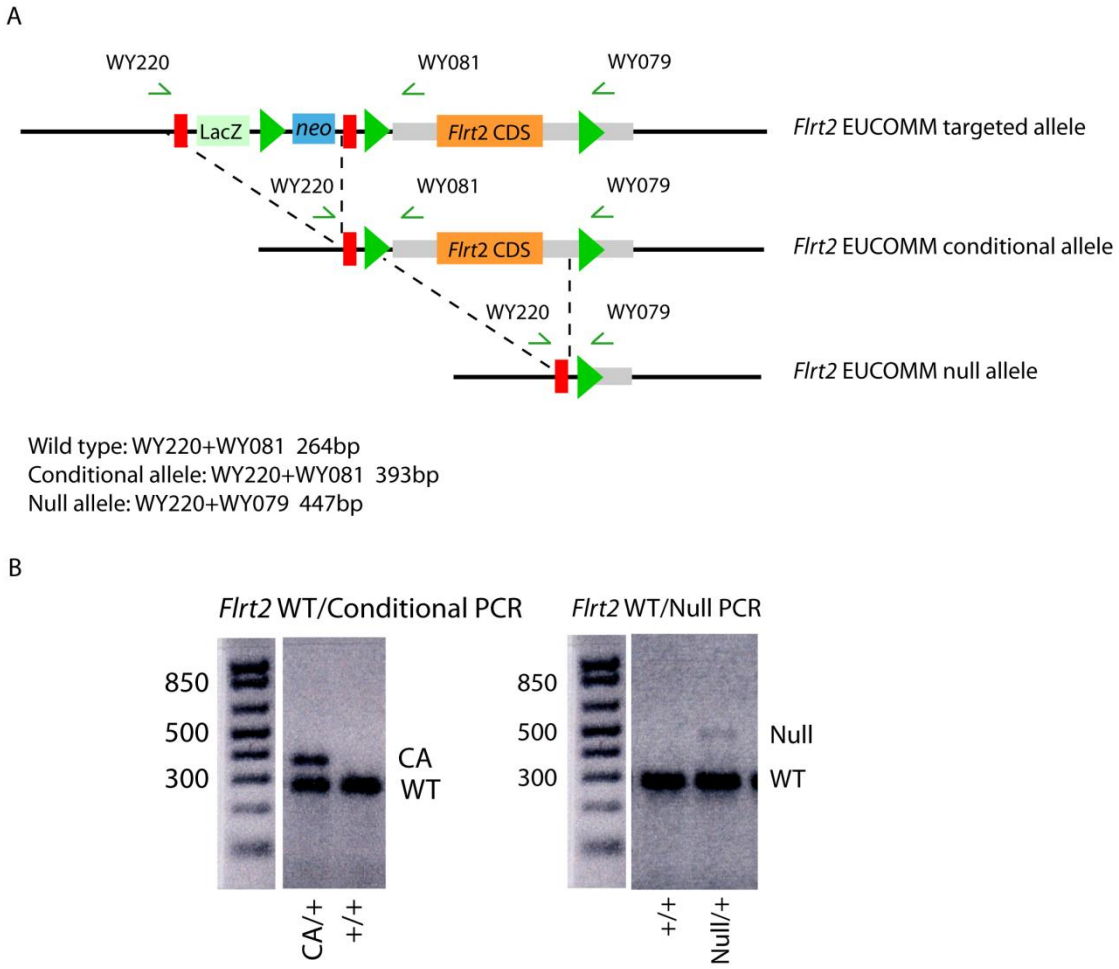


Figure 4.3 Generation of the *Flrt2* conditional and null allele (A) The *Flrt2* conditional allele was generated by FLP recombinase deletion of the *LacZ* sequence (green box) and the neomycin selection cassette (neo, blue box). The *Flrt2* CDS (orange box) was subsequently excised by Cre recombination to generate a *Flrt2* null allele. (B) Representative pictures showing the PCR genotyping of heterozygous *Flrt2* conditional (*Flrt2*$^{CA/+}$) and WT mice (left panel) and also mice after being crossed to *Sox2 Cre Tg*$^{+/-}$ mice (right panel). The primers (green arrows) amplified 264 bp and 393bp products representing the WT and conditional alleles respectively. A 447bp product was produced in the case of a null allele.

4.2.4 Comparison of sites of *Flrt2* expression using the *Flrt2 LacZ* reporter mice

LacZ mRNA expression was examined by a colleague, Dr Kim Cheng, at E9 by whole mount *in situ* hybridisation (WISH) using a probe generated from the *Flrt2* CDS (**Fig 4.4A**) and a probe generated from the *LacZ* CDS (**Fig 4.4B**). Whole embryo detection of functional β-galactosidase (encoded by *LacZ*) was detected using X-gal. As mentioned previously, functional β-galactosidase would indicate sites of *Flrt2* expression, as *LacZ* was driven by the *Flrt2* promoter (**Fig 4.4C**). As shown in **Fig 4.4**, *LacZ* mRNA expression, as detected by WISH, faithfully recapitulated the endogenous expression of *Flrt2* mRNA in mice embryos at E9, in particular, the pro-epicardial organ (PEO), midbrain (MD) and anterior somites (AS). The intensity of staining in all samples were equivalent in the PEO, however, expression in the AS and MD appeared weaker.

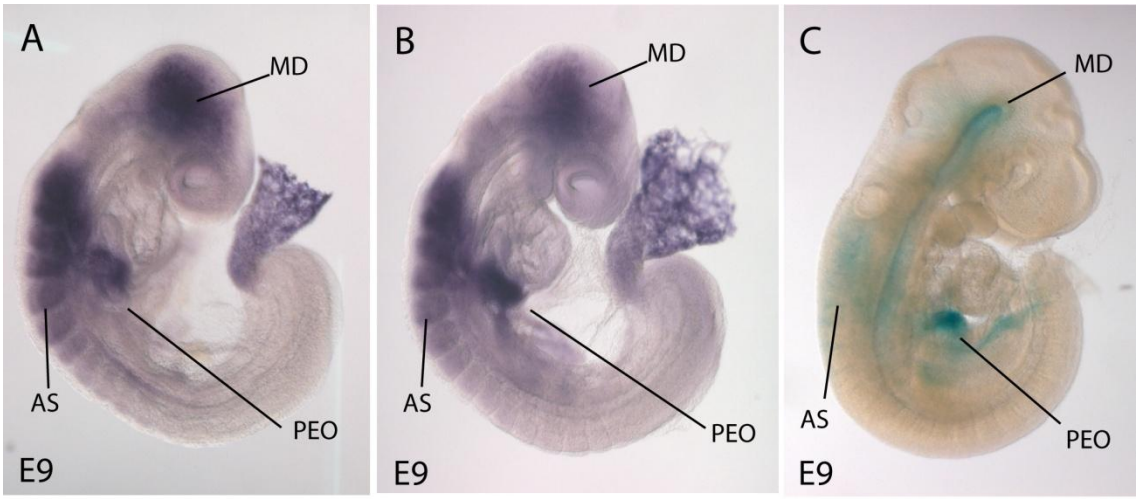


Figure 4.4 Comparison of sites of *Flrt2* expression using the *Flrt2 LacZ* reporter mice. (A) Whole mount *in situ* hybridisation (WISH) of *Flrt2* expression at E9. (B) *Flrt2* promoter initiated *LacZ* expression as detected by WISH at E9. *Flrt2* and *LacZ* expression was detected in the midbrain mesenchyme (MD), anterior somites (AS) and the pro-epicardial organ (PEO). (C) Staining using X-gal at E9 also detected functional β-galactosidase in the PEO and weakly in the MD and AS.

4.3 Expression of *LacZ* in the developing mouse embryo

4.3.1 *Flrt2* promoter driven *LacZ* expression at E9.5

Flrt2 LacZ reporter embryos were collected at E9.5 and stained with X-gal as described in section 4.2.4. As shown in **Fig 4.5A (i-iv)**, whole embryo *LacZ* expression was detected in the MD, PEO and the AS. Stained embryos were cut into 10 µm sections and counterstained with Nuclear Fast Red. Frontal sections of the whole embryo also showed strong localisation of LacZ in the PEO (**Fig 4.5B**).

4.3.2 *Flrt2* promoter driven *LacZ* expression at E10.5

Flrt2 LacZ reporter embryos were collected at E10.5 and stained with X-gal as described in section 4.2.4. At E10.5 *LacZ* expression expanded and became more specific and defined. *LacZ* expression at E10.5 was observed in the MD but unlike embryos at E9.5, LacZ was also observed in the cephalic mesenchyme of the midbrain (**Fig 4.6A**). There was also a clear expression in the maxillary arches which give rise to the palatal shelves that separate the oral cavity from the nasal cavity (**Fig 4.6A**) (Kaufman, 1992). Expression of *LacZ* in the PEO persisted and images suggested that the PEO was starting to migrate towards the heart, ultimately forming the epicardium (**Fig 4.6B**). However, more analysis would be required to confirm this. *LacZ* was also present in the somites and the pancreas (**Fig 4.6B**). Stained embryos were cut into 10 µm sections and counterstained with Nuclear Fast Red. Frontal sections of the whole embryo showed *LacZ* expression in the MD, maxillary arches, PEO, somites and pancreas (**Fig 4.6B**).

4.3.3 *Flrt2* promoter driven *LacZ* expression at E11.5

Flrt2 LacZ reporter embryos were collected at E11.5 and stained with X-gal as described in section 4.2.4. Expression of *LacZ* at E11.5 was present in the cephalic mesenchyme of the midbrain, specifically in the fourth ventricle (FV) of the brain (**Fig 4.7A** and **B**). Expression of *LacZ* was detected in the MA, surface of the heart (H), somites (S), and the pancreas (P) at E11.5 (**Fig 4.7A** and **B**). There is a clear expression of *LacZ* in the intra-retinal space (IR) (**Fig4.7B (iv)**), as one of the most obvious changes at this stage of embryo development is related to the morphology of the cephalic region, particularly in the area around the developing eye (Kaufman, 1992). There was also clear expression of *LacZ* in the pharyngeal arches (PA, **Fig 4.7A**) and the hindlimb buds (HL, **Fig4.7B (v)**).

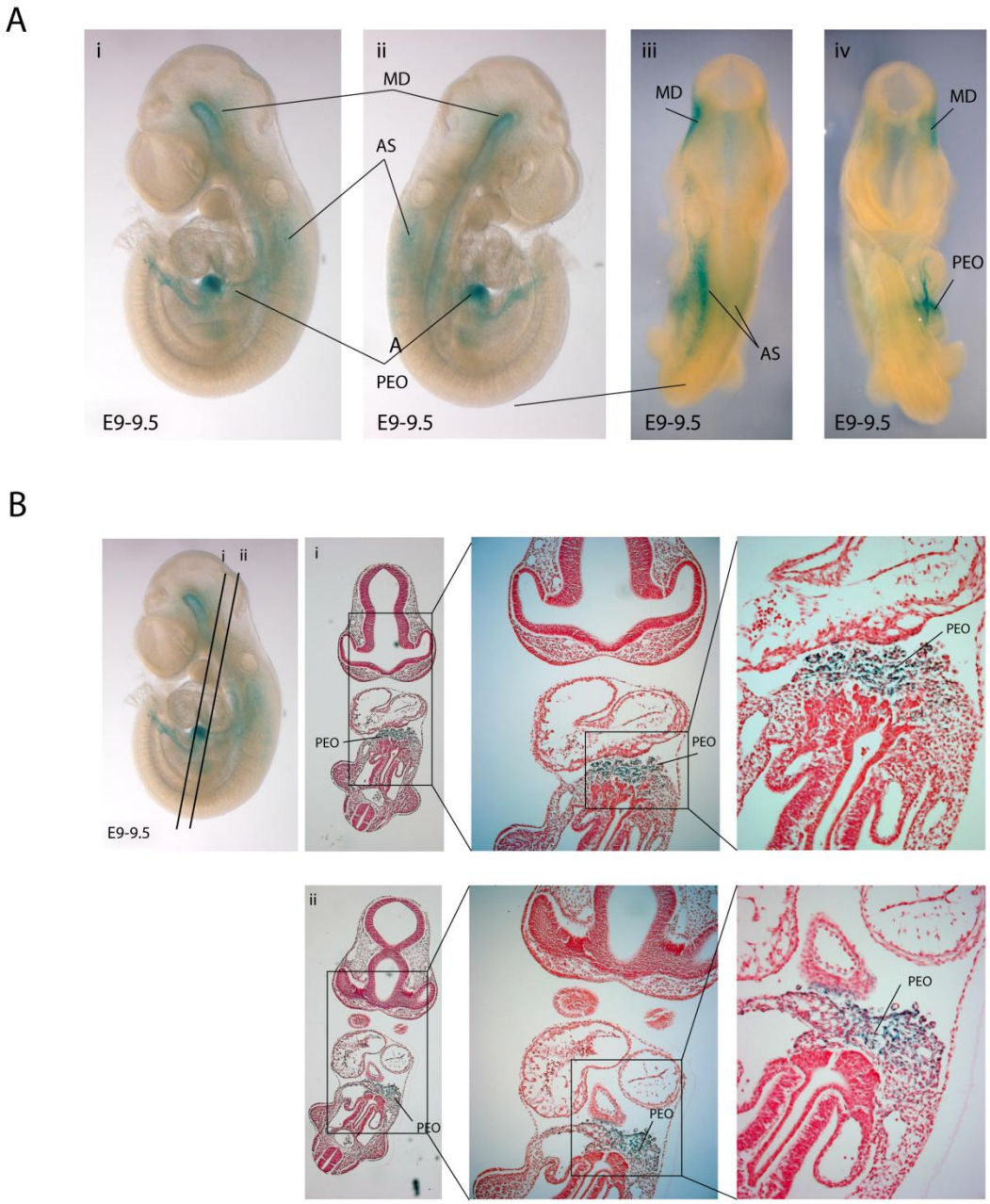


Figure 4.5 *LacZ* expression under the *Flrt2* promoter at E9.5. (A) Representative images of *Flrt2 LacZ* reporter embryos at E9.5. Left and right lateral (i and ii respectively), dorsal (iii) and ventral (iv) orientations are shown. *LacZ* expression was detected in the midbrain (MD), pro-epicardial organ (PEO) and the anterior somites (AS). (B) Frontal sections of *Flrt2 LacZ* reporter embryos clearly showed *LacZ* expression in the PEO (i and ii).

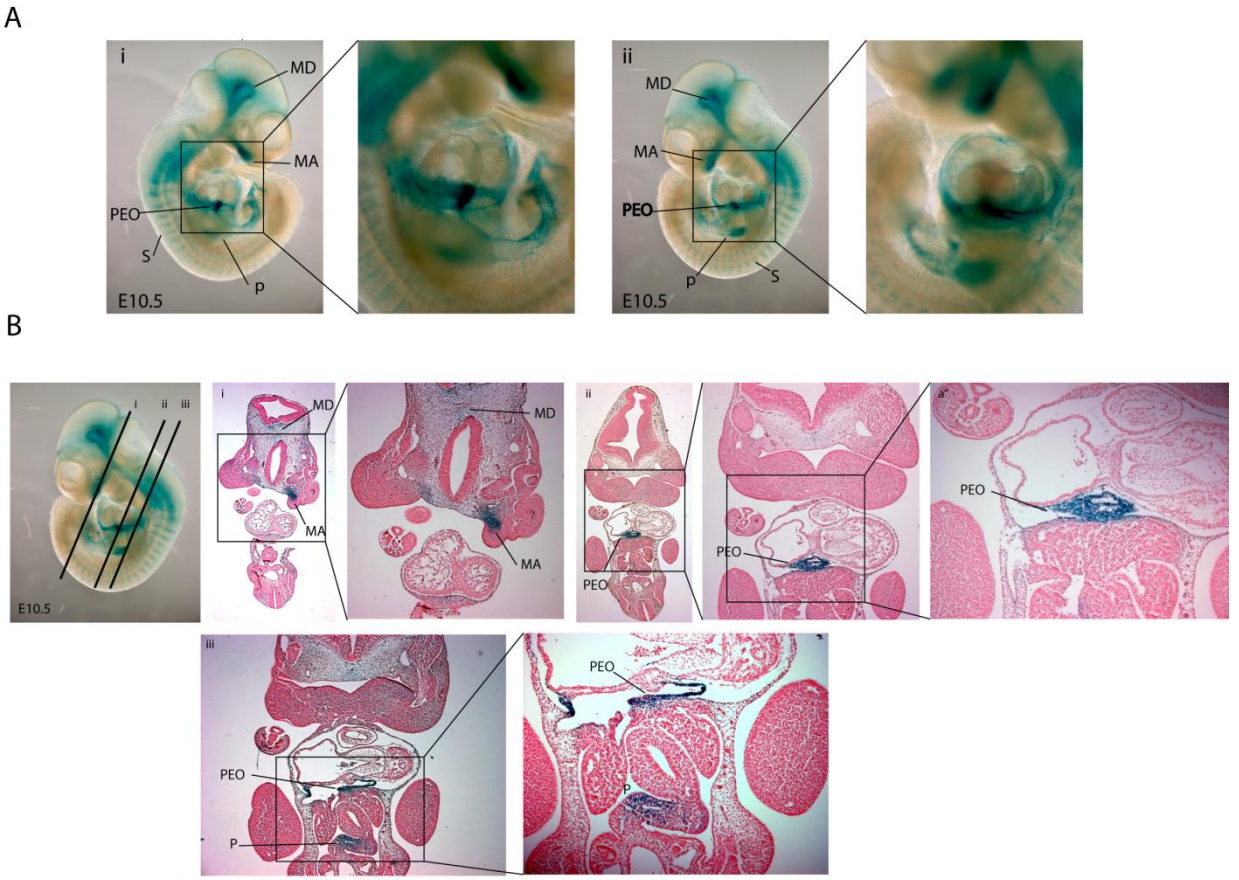


Figure 4.6 *LacZ* expression under the *Flrt2* promoter at E10.5 (A) Representative images from *Flrt2 LacZ* reporter embryos at E10.5 left and right lateral orientations, (i and ii respectively), *LacZ* expression is detectable in the midbrain (MD), maxillary arches (MA), pro-epicardial organ (PEO), somites (s) and pancreas (P). (B) Frontal sections of *Flrt2*$^{LacZ/+}$ embryos showing a clearly visible *LacZ* expression in the cephalic mesenchyme of midbrain and maxillary arches (MA) (i), PEO (ii) and pancreas (iii).

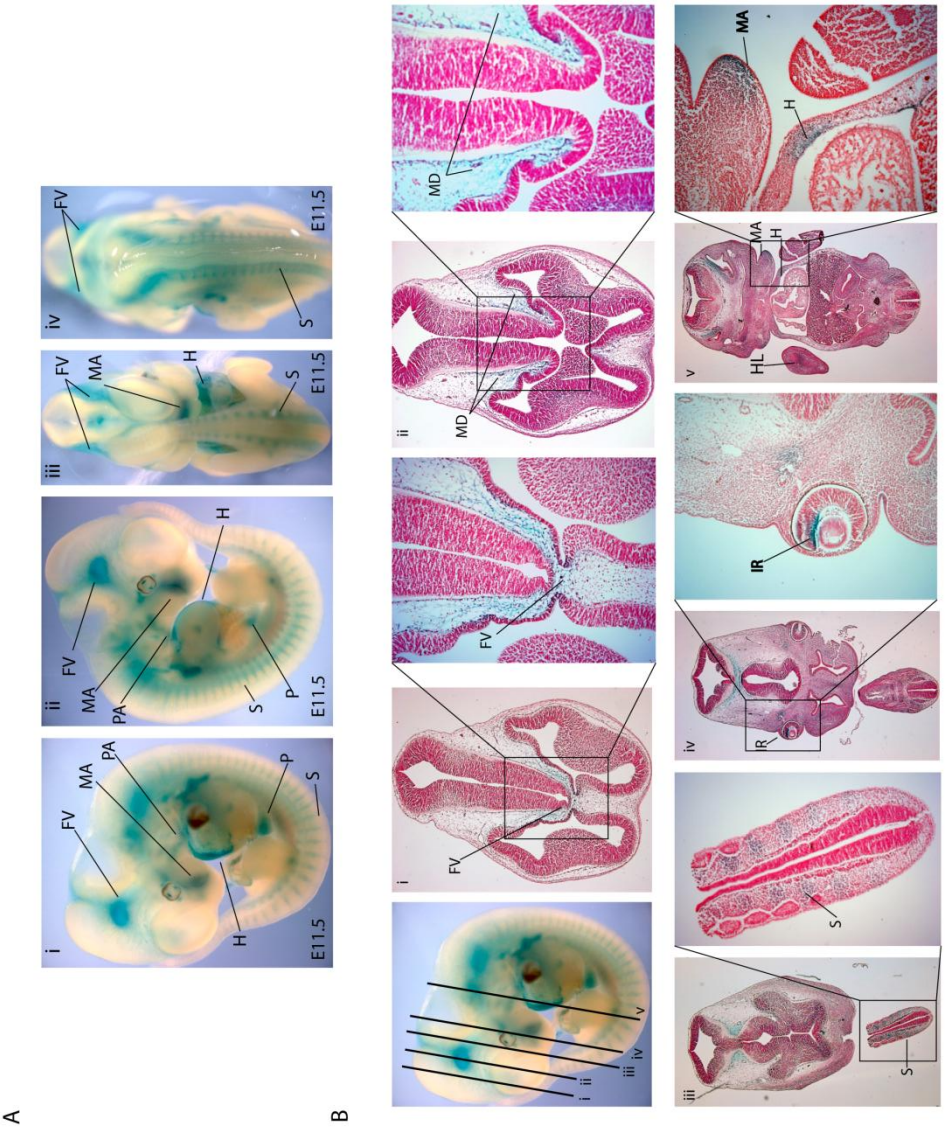


Figure 4.7 LacZ expression under the Flrt2 promoter at E11.6 (A) E11.5 *Flrt2*$^{LacZ/+}$ embryos with left and right lateral (i and ii respectively), dorsal (iii) and ventral (iv) orientations, *LazZ* expression is detectable in the fourth ventricle of the midbrain (FV), maxillary and pharyngeal arches (MA and PA respectively), pro-epicardial organ (PEO), somites (S) and Pancreas (P). (B) Frontal sections of *Flrt2*$^{LacZ/+}$ embryos showing a clearly visible *LacZ* expression in the FV (i), MA (ii), somites (iii), intra-retinal space (IR, iv) and the outer surface of the heart (H) and hindlimb bud (HL) (v, both).

4.4 Conclusion

There is currently no known reporter or conditional *Flrt2* allele described in the literature. *Flrt2* expression sites have been characterised and described (Lacy et al., 1999), and *in vivo* functional activities have been previously studied (Maretto et al., 2008; Muller et al., 2011). The methods used to study sites of *Flrt2* expression such as WISH and histological analysis by immunohistochemistry are time consuming and complicated. The aim of this project was to generate a *Flrt2* reporter and conditional allele to allow further characterisation of *Flrt2* function.

The EUCOMM/KOMP resource *Flrt2* targeted vector was used to generate a *Flrt2* reporter mouse strain carrying the *LacZ* gene. The activity of β-galactosidase (an enzyme encoded by the *LacZ* gene) was used as a tool to detect *Flrt2* expression sites as the *LacZ* gene was driven by the *Flrt2* promoter. In addition, the targeted EUCOMM/KOMP allele allowed the generation of a *Flrt2* conditional allele due to the presence of LoxP sites flanking the *Flrt2* coding sequence.

The results of this chapter showed that generation of *Flrt2 LacZ* reporter mouse strain was possible and it accurately depicted sites of *Flrt2* expression. *Flrt2 LacZ* reporter adult mice were viable and *Flrt2 LacZ* reporter embryos were used to study sites of *Flrt2* expression at different stages of embryonic development (E9.5-E11.5). Reassuringly, the *Flrt2 LacZ* reporter animals confirmed sites of *Flrt2* previously described in the literature (Lacy et al., 1999; Maretto et al., 2008; Muller et al., 2011). Interestingly, the *Flrt2 LacZ* reporter animals also revealed sites of *Flrt2* expression that have not previously been described, such as the intra-retinal space. Taken together, the *Flrt2 LacZ* reporter mouse strain represents a novel and easy to use animal model to

identify sites of *Flrt2* expression. The results of this chapter were only the beginning of a much larger research project, the analysis of which is beyond the scope and time scale of this project.

Another aim of this chapter was to test the fidelity of the *Flrt2* conditional allele. Heterozygous *Flrt2*$^{CA/+}$ adult mice were viable and the small number of embryo samples collected (after *Sox 2 Cre* recombinase excision) revealed the absence of any embryos of the *Flrt2*$^{-/-}$ genotype. Despite the small sample size, results would suggest that in the presence of *Sox2 Cre* recombinase, the Flrt2 CDS was excised, creating a null allele and causing embryonic lethality. However, the number of embryos collected was not sufficient for statistical analysis (24 embryos of which 15 were wild type and 9 were heterzygoute mutants) and additional *Flrt2*$^{+/-}$ intercrosses are currently ongoing.

Chapter 5

General discussion

5.1 Introduction

The experiments performed in this thesis were designed to achieve two goals, first to examine a genetic hypothesis that closely related members of the fibronectin leucine-rich repeat transmembrane (Flrt) protein family, namely *Flrt2* and *Flrt3,* were functioning cooperatively in sites of co-expression. The second goal was to generate a *Flrt2 LacZ* reporter and a *Flrt2* conditional allele to further investigate sites of *Flrt2* expression and function in the developing mouse embryo.

As detailed in chapter 1, adhesion molecules, such as those in the Flrt family of proteins, play crucial roles in interactions between various tissues and their surrounding cells during embryo morphogenesis (Barone and Heisenberg, 2012). The Flrt family of proteins were reported to be expressed in different tissues and organs in humans (Lacy et al., 1999). *In vivo* functional activities of all three Flrt proteins in mouse embryo were previously studied in this laboratory (Maretto et al., 2008; Muller et al., 2011). Flrt proteins were also found to be involved in various signalling pathways and processes throughout mouse embryonic development. It was recently published that Flrt proteins function as endogenous ligands to other proteins involved in regulating the developing central nervous system (O'Sullivan et al., 2012; Robinson et al., 2004; Yamagishi et al., 2011).

Flrt2 and *Flrt3* were shown to be co-expressed in several tissue sites in mouse embryos (Egea et al., 2008; Maretto et al., 2008; Muller et al., 2011). Mice lacking *Flrt2* had defects in the integrity of the epicardial tissue layer in the developing heart, resembling the defects in the basement membrane (BM) of the anterior visceral endoderm (AVE) caused by loss of *Flrt3* (Muller et a*l., 2011)*. *Flrt2* and *Flrt3* were reported to play conserved functional roles in

maintaining cell-cell contacts in the epicardium and AVE respectively (Muller et al., 2011). The hypothesis for the first part of this project was that mice lacking both *Flrt2* and *Flrt3* were embryonic lethal due to a lack of compensatory mechanism. This was achieved by generating *Flrt2*$^{-/-}$*; Flrt3*$^{-/-}$ mice through a complicated breeding strategy as outline in Chapter 3.

The second part of this project was to generate a *Flrt2* reporter mouse strain and also a mouse strain capable of tissue specific conditional deletion of *Flrt2*. *Flrt2* expression patterns have previously been studied using whole embryo *in situ* hybridisation and immunohistochemistry methods (Haines et al., 2006; Muller et al., 2011). The "knockout-first" allele designed by the EUCOMM/KOMP resource (Bradley et al., 2012; Skarnes et al.), allowed for successful generation of a *Flrt2 LacZ* reporter and conditional mouse strains. The *Flrt2 LacZ* reporter mouse strain was used as a useful tool to verify *Flrt2* expression sites, whereas the *Flrt2* conditional mouse strain will be a useful tool to further characterise Flrt2 function.

5.2 Mice lacking *Flrt2* and *Flrt3* were embryonic lethal

The genetic experiment, performed and detailed in chapter 3, confirmed the hypothesis that mice lacking both *Flrt2* and *Flrt3* were unable to survive past gestation and were embryonic lethal. The percentage of *Flrt2*$^{-/-}$*; Flrt3*$^{-/-}$ embryos collected at E10.5 were statistically significant to that of the expected (3% observed vs. 6.25% expected), whereas the percentages of *Flrt2*$^{-/-}$ and *Flrt3*$^{-/-}$ single mutant embryos were unaffected (18.8% and 17.5% observed respectively vs. 18.75% expected). Interestingly, *Flrt2*$^{-/-}$*; Flrt3*$^{-/-}$ embryos collected at E9.5 correctly followed the expected Mendelian ratio (6.8% observed vs. 6.25 expected).

During the heart development in mouse embryo, between E9.5 and E10.5, the neural crest, one of the three heart progenitor cells, the other two being cardiac mesoderm and the PEO, migrate into the outflow tract of the heart to help remodelling and separation of the heart arteries (Jiang et al., 2000). The PEO gives rise to the epicardium that attaches and surrounds the myocardium (the middle of the three layers forming the wall of the heart). The PEO is involved in proliferation and diversification of the heart development (for a review, see (Manner et al., 2001). *Flrt2* and *Flrt3* show overlapping expression domains in the PEO up until E10, when the PEO starts to form the epicardial cells that attach and migrate onto the surface of the heart. After E10 Flrt3 expression was downregulated in the epicardium, and only *Flrt2* expression maintained (Muller et al., 2011). Global loss of *Flrt3* in mice resulted in embryonic lethality by E10.5 (Maretto et al., 2008) and *Flrt2*$^{-/-}$ embryos die between E11.5-E12.5 (Muller et al., 2011). *Sox2 Cre* deletion of the *Flrt2* Hygro allele produced viable mice.

Flt2$^{-/-}$*; Flrt3*$^{-/-}$ embryos die at E10.5, the same stage when the structural defect of the AVE and disruption of the BM of the *Flrt3*$^{-/-}$ embryos causes lethality. The double mutant embryos failed to develop beyond E10.5 when both *Flrt2* and *Flrt3* were lost. The requirement of *Flrt3* in the AVE of the *Flrt2*$^{-/-}$*; Flrt3*$^{-/-}$ embryos was by-passed by using *Sox2 Cre* deletion of *Flrt3* in the embryo only, not in the extraembryonic tissues. It seems *Flrt3* was playing a compensation role since the *Flrt2*$^{-/-}$ embryo die at later stage (E11.5 - E12.5) when *Flrt3* was present, and failed to develop beyond E10.5 when *Flrt3* was lost Obviously there could be other reasons causing embryonic lethality of *Flrt2*$^{-/-}$*; Flrt3*$^{-/-}$ mice such as other interacting molecules or proteins that act directly or indirectly to affect signalling pathways initiated by either or both of *Flrt2* and

Flrt3. Both genes are downstream target of Nodal/TGF-β signalling pathway, and interruption of the signalling pathway can also be of fatal consequences, but that is beyond the scope and experimental range designed for this project.

5.3 *Flrt2 LacZ* reporter and *Flrt2* conditional allele are useful tools for dissecting *Flrt2* expression domains

As outlined in Chapter 4, an easy to use *Flrt2* reporter mouse strain would be extremely useful in identifying *Flrt2* expression domains. The *Flrt2 LacZ* reporter mice were generated from the targeted EUCOMM/KOMP allele resource and these mice provided a reliable depiction of endogenous *Flrt2* mRNA expression at all stages of embryonic development collected. The inconsistency between the WISH and LacZ staining noticed in some of the results detailed in chapter 3 could be due to the method of staining. A recent report provided an alternative β-Galactosidase detection method when X-gal failed to detect staining in embryos from LacZ-based transgenic mouse strains (Sundararajan et al., 2012), The use of Salmon-gal in combination with tetrazolium salts provided more sensitive and fast reaction than β-Galactosidase assay in mouse embryos.

A mouse strain allowing for tissue specific deletion of *Flrt2* was also generated, as detailed in Chapter 4. The *Flrt2* conditional mouse strain can be used in further experiments to investigate the effect of deleting *Flrt2* in particular sites or organs, as this is technically difficult in whole body knockouts of *Flrt2*.

5.4 Outlook and further experiments

Based on results outlined in Chapter 3, mice lacking both *Flrt2* and *Flrt3* seem to have a more severe phenotype than deletion of *Flrt2* or *Flrt3* alone. The

results of this project were unable to determine the cause of embryonic lethality in *Flrt2*$^{-/-}$*; Flrt3*$^{-/-}$ animals and further analysis will need to be performed. The PEO is important for differentiation and diversification of the developing heart, and similar abnormalities were observed in single deletions of *Flrt2* and *Flrt3* (Egea et al., 2008; Maretto et al., 2008; Muller et al., 2011). It would thus be reasonable to assume that there are abnormalities in PEO formation in the *Flrt2*$^{-/-}$*; Flrt3*$^{-/-}$ mice and therefore provide an initial entry point for analysis. Future work can involve histological analysis of the PEO at different stages of embryonic development, using molecular markers specific to the PEO, such as Scleraxis (Scx) and Semaphorin3D (Sema3D) that genetically delineate uncharacterised PEO subcompartments (Katz et al., 2012). Histology sections of the *Flrt2*$^{-/-}$*; Flrt3*$^{-/-}$ whole embryos can be compared to *Flrt2*$^{-/-}$ and *Flrt3*$^{-/-}$ single mutants to identify any morphological differences.

Since the *Flrt2* conditional allele successfully generated *Flrt2* null allele, it will be interesting to test for functional lethality of the *Flrt2*$^{-/-}$ embryos compared to those described in Muller and colleagues which die between E11.5-E12.5 (Muller et al., 2011). The *Flrt2* conditional allele can also be used to analyse tissue or organ specific deletion of *Flrt2*. Flrt2 was shown to be strongly expressed in human pancreas (Lacy et al., 1999), but little is known regarding its function. Several pancreas specific Cre recombinase strains are available and have previously been described in the literature. For example, the rat insulin promoter (*RIP)-Cre* mice strain carries a transgene construct containing the rat insulin II promoter and thus any Cre recombinase activity is limited to insulin expressing cells (Lee et al., 2006; Postic et al., 1999). Another pancreas specific Cre recombinase is the pancreatic and duodenal homeobox-1 (*Pdx1) Cre*. This mouse strain exhibits a stochastic pattern of high level Cre expression

in the pancreas driven by the *Pdx1* promoter, *Pdx1* being of one of the earliest detectable transcription factors in the pancreas and is essential for pancreas development (Hingorani et al., 2003). The Pdx1 Cre mice strain can be used to dissect *Flrt2* function in the entire pancreas.

Overall, the results from this thesis have added to our understanding of Flrt2 and Flrt3 functional redundancy, compensational roles and expression patterns in mouse embryo. The strains generated will be important for delineating the functions of Flrt2 and Flrt3 but further work will need to be performed to analyse the nature of the defect resulting from losing both genes in the mouse embryo.

Chapter 6

References

Arnold, S.J., and Robertson, E.J. (2009). Making a commitment: cell lineage allocation and axis patterning in the early mouse embryo. Nat Rev Mol Cell Biol *10*, 91-103.

Arnold, S.J.a.R., E. J. (2006). Dose-dependent Smad1, Smad5 and Smad8 signaling in the early mouse embryo. Dev Biol *296*, 104-118.

Barone, V., and Heisenberg, C.P. (2012). Cell adhesion in embryo morphogenesis. Curr Opin Cell Biol *24*, 148-153.

Beddington, R.S., and Robertson, E.J. (1999). Axis development and early asymmetry in mammals. Cell *96*, 195-209.

Bell, J.K., Botos, I., Hall, P.R., Askins, J., Shiloach, J., Segal, D.M., and Davies, D.R. (2005). The molecular structure of the Toll-like receptor 3 ligand-binding domain. Proc Natl Acad Sci U S A *102*, 10976-10980.

Blaber, M., DiSalvo, J., and Thomas, K.A. (1996). X-ray crystal structure of human acidic fibroblast growth factor. Biochemistry *35*, 2086-2094.

Bottcher, R.T., Pollet, N., Delius, H., and Niehrs, C. (2004). The transmembrane protein XFLRT3 forms a complex with FGF receptors and promotes FGF signalling. Nat Cell Biol *6*, 38-44.

Bradley, A., Anastassiadis, K., Ayadi, A., Battey, J.F., Bell, C., Birling, M.C., Bottomley, J., Brown, S.D., Burger, A., Bult, C.J.*, et al.* The mammalian gene function resource: the international knockout mouse consortium. Mamm Genome *23*, 580-586.

Bradley, A., Anastassiadis, K., Ayadi, A., Battey, J.F., Bell, C., Birling, M.C., Bottomley, J., Brown, S.D., Burger, A., Bult, C.J.*, et al.* (2012). The mammalian gene function resource: the international knockout mouse consortium. Mamm Genome *23*, 580-586.

Brand, T. (2003). Heart development: molecular insights into cardiac specification and early morphogenesis. Dev Biol *258*, 1-19.

Cascio, S., and Zaret, K.S. (1991). Hepatocyte differentiation initiates during endodermal-mesenchymal interactions prior to liver formation. Development *113*, 217-225.

Chang, H., Huylebroeck, D., Verschueren, K., Guo, Q., Matzuk, M.M., and Zwijsen, A. (1999). Smad5 knockout mice die at mid-gestation due to multiple embryonic and extraembryonic defects. Development *126*, 1631-1642.

De Langhe, S.P., Carraro, G., Tefft, D., Li, C., Xu, X., Chai, Y., Minoo, P., Hajihosseini, M.K., Drouin, J., Kaartinen, V.*, et al.* (2008). Formation and differentiation of multiple mesenchymal lineages during lung development is regulated by beta-catenin signaling. PLoS One *3*, e1516.

Dolan, J., Walshe, K., Alsbury, S., Hokamp, K., O'Keeffe, S., Okafuji, T., Miller, S.F., Tear, G., and Mitchell, K.J. (2007). The extracellular leucine-rich repeat superfamily; a comparative survey and analysis of evolutionary relationships and expression patterns. BMC Genomics *8*, 320.

Egea, J., Erlacher, C., Montanez, E., Burtscher, I., Yamagishi, S., Hess, M., Hampel, F., Sanchez, R., Rodriguez-Manzaneque, M.T., Bosl, M.R.*, et al.* (2008). Genetic ablation of FLRT3 reveals a novel morphogenetic function for the anterior visceral endoderm in suppressing mesoderm differentiation. Genes Dev *22*, 3349-3362.

Hackett, B.P. (2002). Formation and malformation of the vertebrate left-right axis. Curr Mol Med *2*, 39-66.

Haines, B.P., Wheldon, L.M., Summerbell, D., Heath, J.K., and Rigby, P.W. (2006). Regulated expression of FLRT genes implies a functional role in the regulation of FGF signalling during mouse development. Dev Biol *297*, 14-25.

Harvey, R.P. (1999). Seeking a regulatory roadmap for heart morphogenesis. Semin Cell Dev Biol *10*, 99-107.

Harvey, R.P. (2002). Patterning the vertebrate heart. Nat Rev Genet *3*, 544-556.

Haupt, S., Edenhofer, F., Peitz, M., Leinhaas, A., and Brustle, O. (2007). Stage-specific conditional mutagenesis in mouse embryonic stem cell-derived neural cells and postmitotic neurons by direct delivery of biologically active Cre recombinase. Stem Cells *25*, 181-188.

Hayashi, S., Lewis, P., Pevny, L., and McMahon, A.P. (2002). Efficient gene modulation in mouse epiblast using a Sox2Cre transgenic mouse strain. Mech Dev *119 Suppl 1*, S97-S101.

Hingorani, S.R., Petricoin, E.F., Maitra, A., Rajapakse, V., King, C., Jacobetz, M.A., Ross, S., Conrads, T.P., Veenstra, T.D., Hitt, B.A.*, et al.* (2003). Preinvasive and invasive ductal pancreatic cancer and its early detection in the mouse. Cancer Cell *4*, 437-450.

Hiruma, T., and Hirakow, R. (1989). Epicardial formation in embryonic chick heart: computer-aided reconstruction, scanning, and transmission electron microscopic studies. Am J Anat *184*, 129-138.

Hussain, M.M., Rava, P., Walsh, M., Rana, M., and Iqbal, J. (2012). Multiple functions of microsomal triglyceride transfer protein. Nutr Metab (Lond) *9*, 14.

Jiang, X., Rowitch, D.H., Soriano, P., McMahon, A.P., and Sucov, H.M. (2000). Fate of the mammalian cardiac neural crest. Development *127*, 1607-1616.

Kajava, A.V. (1998). Structural diversity of leucine-rich repeat proteins. J Mol Biol *277*, 519-527.

Karaulanov, E.E., Bottcher, R.T., and Niehrs, C. (2006). A role for fibronectin-leucine-rich transmembrane cell-surface proteins in homotypic cell adhesion. EMBO Rep *7*, 283-290.

Katz, T.C., Singh, M.K., Degenhardt, K., Rivera-Feliciano, J., Johnson, R.L., Epstein, J.A., and Tabin, C.J. (2012). Distinct compartments of the proepicardial organ give rise to coronary vascular endothelial cells. Dev Cell *22*, 639-650.

Kobe, B., and Kajava, A.V. (2001). The leucine-rich repeat as a protein recognition motif. Curr Opin Struct Biol *11*, 725-732.

Lacy, S.E., Bonnemann, C.G., Buzney, E.A., and Kunkel, L.M. (1999). Identification of FLRT1, FLRT2, and FLRT3: a novel family of transmembrane leucine-rich repeat proteins. Genomics *62*, 417-426.

Lee, J.Y., Ristow, M., Lin, X., White, M.F., Magnuson, M.A., and Hennighausen, L. (2006). RIP-Cre revisited, evidence for impairments of pancreatic beta-cell function. J Biol Chem *281*, 2649-2653.

Lu, C.C., Brennan, J., and Robertson, E.J. (2001). From fertilization to gastrulation: axis formation in the mouse embryo. Curr Opin Genet Dev *11*, 384-392.

Manner, J., Perez-Pomares, J.M., Macias, D., and Munoz-Chapuli, R. (2001). The origin, formation and developmental significance of the epicardium: a review. Cells Tissues Organs *169*, 89-103.

Maretto, S., Muller, P.S., Aricescu, A.R., Cho, K.W., Bikoff, E.K., and Robertson, E.J. (2008). Ventral closure, headfold fusion and definitive endoderm migration defects in mouse embryos lacking the fibronectin leucine-rich transmembrane protein FLRT3. Dev Biol *318*, 184-193.

Mikawa, T., and Gourdie, R.G. (1996). Pericardial mesoderm generates a population of coronary smooth muscle cells migrating into the heart along with ingrowth of the epicardial organ. Dev Biol *174*, 221-232.

Muller, P.S., Schulz, R., Maretto, S., Costello, I., Srinivas, S., Bikoff, E., and Robertson, E. (2011). The fibronectin leucine-rich repeat transmembrane protein Flrt2 is required in the epicardium to promote heart morphogenesis. Development *138*, 1297-1308.

Nielsen, L.B., Perko, M., Arendrup, H., and Andersen, C.B. (2002). Microsomal triglyceride transfer protein gene expression and triglyceride accumulation in hypoxic human hearts. Arterioscler Thromb Vasc Biol *22*, 1489-1494.

Nonaka, S., Yoshiba, S., Watanabe, D., Ikeuchi, S., Goto, T., Marshall, W.F., and Hamada, H. (2005). De novo formation of left-right asymmetry by posterior tilt of nodal cilia. PLoS Biol *3*, e268.

O'Sullivan, M.L., de Wit, J., Savas, J.N., Comoletti, D., Otto-Hitt, S., Yates, J.R., 3rd, and Ghosh, A. (2012). FLRT proteins are endogenous latrophilin ligands and regulate excitatory synapse development. Neuron *73*, 903-910.

Ogata, S., Morokuma, J., Hayata, T., Kolle, G., Niehrs, C., Ueno, N., and Cho, K.W. (2007). TGF-beta signaling-mediated morphogenesis: modulation of cell adhesion via cadherin endocytosis. Genes Dev *21*, 1817-1831.

Perea-Gomez, A., Vella, F.D., Shawlot, W., Oulad-Abdelghani, M., Chazaud, C., Meno, C., Pfister, V., Chen, L., Robertson, E., Hamada, H.*, et al.* (2002). Nodal antagonists in the anterior visceral endoderm prevent the formation of multiple primitive streaks. Dev Cell *3*, 745-756.

Postic, C., Shiota, M., Niswender, K.D., Jetton, T.L., Chen, Y., Moates, J.M., Shelton, K.D., Lindner, J., Cherrington, A.D., and Magnuson, M.A. (1999). Dual roles for glucokinase in glucose homeostasis as determined by liver and pancreatic beta cell-specific gene knock-outs using Cre recombinase. J Biol Chem *274*, 305-315.

Rathjen, J., Lake, J.A., Bettess, M.D., Washington, J.M., Chapman, G., and Rathjen, P.D. (1999). Formation of a primitive ectoderm like cell population, EPL cells, from ES cells in response to biologically derived factors. J Cell Sci *112 (Pt 5)*, 601-612.

Robertson, E.J., Norris, D.P., Brennan, J., and Bikoff, E.K. (2003). Control of early anterior-posterior patterning in the mouse embryo by TGF-beta signalling. Philos Trans R Soc Lond B Biol Sci *358*, 1351-1357; discussion 1357.

Robinson, M., Parsons Perez, M.C., Tebar, L., Palmer, J., Patel, A., Marks, D., Sheasby, A., De Felipe, C., Coffin, R., Livesey, F.J.*, et al.* (2004). FLRT3 is expressed in sensory neurons after peripheral nerve injury and regulates neurite outgrowth. Mol Cell Neurosci *27*, 202-214.

Rodriguez, T.A., Srinivas, S., Clements, M.P., Smith, J.C., and Beddington, R.S. (2005). Induction and migration of the anterior visceral endoderm is regulated by the extra-embryonic ectoderm. Development *132*, 2513-2520.

Rossant, J., and Tam, P.P. (2004). Emerging asymmetry and embryonic patterning in early mouse development. Dev Cell *7*, 155-164.

Rossi, J.M., Dunn, N.R., Hogan, B.L., and Zaret, K.S. (2001). Distinct mesodermal signals, including BMPs from the septum transversum mesenchyme, are required in combination for hepatogenesis from the endoderm. Genes Dev *15*, 1998-2009.

Skarnes, W.C., Rosen, B., West, A.P., Koutsourakis, M., Bushell, W., Iyer, V., Mujica, A.O., Thomas, M., Harrow, J., Cox, T.*, et al.* A conditional knockout resource for the genome-wide study of mouse gene function. Nature *474*, 337-342.

Skarnes, W.C., Rosen, B., West, A.P., Koutsourakis, M., Bushell, W., Iyer, V., Mujica, A.O., Thomas, M., Harrow, J., Cox, T.*, et al.* (2011). A conditional knockout resource for the genome-wide study of mouse gene function. Nature *474*, 337-342.

Smith, T.G., and Tickle, C. (2006). The expression of Flrt3 during chick limb development. Int J Dev Biol *50*, 701-704.

Sollner, C., and Wright, G.J. (2009). A cell surface interaction network of neural leucine-rich repeat receptors. Genome Biol *10*, R99.

Sundararajan, S., Wakamiya, M., Behringer, R.R., and Rivera-Perez, J.A. (2012). A fast and sensitive alternative for beta-galactosidase detection in mouse embryos. Development *139*, 4484-4490.

Tam, P.P., and Behringer, R.R. (1997). Mouse gastrulation: the formation of a mammalian body plan. Mech Dev *68*, 3-25.

Tam, P.P., and Trainor, P.A. (1994). Specification and segmentation of the paraxial mesoderm. Anat Embryol (Berl) *189*, 275-305.

Varlet, I., Collignon, J., and Robertson, E.J. (1997). nodal expression in the primitive endoderm is required for specification of the anterior axis during mouse gastrulation. Development *124*, 1033-1044.

Wetterau, J.R., and Zilversmit, D.B. (1984). A triglyceride and cholesteryl ester transfer protein associated with liver microsomes. J Biol Chem *259*, 10863-10866.

Yamagishi, S., Hampel, F., Hata, K., Del Toro, D., Schwark, M., Kvachnina, E., Bastmeyer, M., Yamashita, T., Tarabykin, V., Klein, R.*, et al.* (2011). FLRT2 and FLRT3 act as repulsive guidance cues for Unc5-positive neurons. EMBO J *30*, 2920-2933.

Yang, X., Castilla, L.H., Xu, X., Li, C., Gotay, J., Weinstein, M., Liu, P.P., and Deng, C.X. (1999). Angiogenesis defects and mesenchymal apoptosis in mice lacking SMAD5. Development *126*, 1571-1580.

Zaret, K.S. (2001). Hepatocyte differentiation: from the endoderm and beyond. Curr Opin Genet Dev *11*, 568-574.